Sources and Transport Pathways of Precipitating Waters in Cold-Season Deep North Atlantic Cyclones

LUKAS PAPRITZ,[a] FRANZISKA AEMISEGGER,[a] AND HEINI WERNLI[a]

[a] *Institute for Atmospheric and Climate Science, ETH Zurich, Zurich, Switzerland*

(Manuscript received 15 April 2021, in final form 26 July 2021)

ABSTRACT: Extratropical cyclones are responsible for a large share of precipitation at midlatitudes and they profoundly impact the characteristics of the water cycle. In this study, we use the ERA5 and a cyclone tracking scheme combined with a Lagrangian diagnostic to identify the sources of moisture precipitating close to the center of 676 deep North Atlantic cyclones in winters 1979–2018. Moisture uptakes occur predominantly in originally cold and dry air heated over the North Atlantic, in particular, over the warm waters of the Gulf Stream, whereas more remote sources from land or the subtropics are less important. Analyzing the dynamical environment of moisture uptakes, we find that moisture precipitating during the cyclone intensification phase originates in the precyclone environment in the cold sectors of preceding cyclones and the cyclone–anticyclone interaction zone. These moisture uptakes are linked to the cyclone's ascent regions via the so-called feeder airstream, a northeasterly cyclone-relative flow that arises due to the cyclone propagation exceeding the advection by the low-level background flow. During the decay phase, more and more of the moisture originates in the cyclone's own cold sector. Consequently, the residence time of precipitating waters in cyclones is short (median of ≈2 days) and transport distances are typically less than the distance traveled by the cyclone itself. These findings emphasize the importance of preconditioning by surface fluxes in the precyclone environment for the formation of precipitation in cyclones and suggest an important role for the hand-over of moisture from one cyclone to the next within a storm track.

KEYWORDS: North Atlantic Ocean; Lagrangian circulation/transport; Trajectories; Extratropical cyclones; Precipitation; Moisture/moisture budget

1. Introduction

Extratropical cyclones play a key role in the atmospheric water cycle and in shaping its characteristics. They are the main precipitation generating weather system at midlatitudes (Hawcroft et al. 2012; Papritz et al. 2014) and concomitant with their attendant fronts they account for more than 80% of the precipitation extremes in the storm track regions (Pfahl and Wernli 2012; Catto and Pfahl 2013; Pfahl et al. 2014). In addition, they transport moisture from lower latitudes poleward (e.g., Peixoto and Oort 1992) and variations in their frequency and tracks have a strong impact on the moisture budget of the polar regions (e.g., Sorteberg and Walsh 2008; Dufour et al. 2016; Naakka et al. 2019). Even though cyclones are an important sink of atmospheric moisture, the redistribution of air by the cyclone circulation is also a driver of intense evaporation from the ocean surface, for instance, via the advection of polar cold air over a warm ocean and strong near-surface winds (e.g., Reed and Albright 1986; Nuss 1989; Zolina and Gulev 2003; Papritz et al. 2015; Vannière et al. 2017; Tilinina et al. 2018) or by entraining dry air from aloft into the planetary boundary layer within the so-called dry intrusion (Raveh-Rubin 2017). Consequently, cyclones can act as a net source of moisture in the atmospheric boundary layer and leave behind a filament of humid air (Dacre et al. 2015, 2019) that can eventually be tapped by subsequent cyclones (Sodemann and Stohl 2013). These rich and varied influences of cyclones on evaporation, moisture transport, and precipitation reveal a complex and yet not fully understood role of cyclones in the atmospheric water cycle. Our goal in this study is to shed light on some specific aspects of the cyclone-related water cycle, namely, the origin, uptake characteristics, and transport pathways of moisture that precipitates close to the center of North Atlantic cyclones.

Cyclones do not only modulate the water cycle but their dynamical evolution is also strongly affected by moist processes, providing further motivation for our study. Latent heat release during condensation contributes substantially to the (rapid) intensification of cyclones via the diabatic production of potential vorticity in the lower troposphere (Uccellini 1990; Reed et al. 1992; Stoelinga 1996; Rossa et al. 2000; Čampa and Wernli 2012; Ludwig et al. 2014; Binder et al. 2016). Furthermore, it enhances the poleward propagation of cyclones and, thus, influences their tracks (Coronel et al. 2015; Tamarin and Kaspi 2016). Even though substantial amounts of precipitation can fall along elongated (cold) fronts of cyclones (Catto et al. 2012; Papritz et al. 2014), the bulk of precipitation falls in the warm sector to the northeast of the cyclone center (Chang and Song 2006; Field and Wood 2007; Rudeva and Gulev 2011) and is closely linked to cross-isentropic ascent of air from the boundary layer to the upper troposphere, mainly along the so-called cyclonic branch of the warm conveyor belt (Browning 1990; Wernli 1997). It is in these locations where diabatic heating unfolds its strongest influence on the dynamical evolution of cyclones (e.g., Stoelinga 1996; Madonna et al.

Supplemental information related to this paper is available at the Journals Online website: https://doi.org/10.1175/JAS-D-21-0105.s1.

Corresponding author: Lukas Papritz, lukas.papritz@env.ethz.ch

DOI: 10.1175/JAS-D-21-0105.1

2014; Binder et al. 2016). For this reason we will focus on precipitation in the core regions of cyclones and disregard precipitation that falls more remotely with respect to the cyclone center such as along trailing cold fronts.

To pinpoint the moisture sources of cyclone precipitation, it is instructive to first consider the climatologically dominant oceanic evaporation regions. They are collocated with the subtropical anticyclones as well as with the warm ocean currents such as the Gulf Stream and the Kuroshio (e.g., Trenberth and Guillemot 1998). Often narrow plumes of high vertically integrated water vapor, sometimes termed atmospheric rivers, extend from the subtropics deep into midlatitudes (cf. Sodemann et al. 2020, and references therein). Knippertz and Wernli (2010) showed that the rapidly intensifying and devastating Storm Klaus, whose intensification was strongly amplified by latent heat release (Fink et al. 2012), formed in a region with very humid air that originated in the tropics. This suggests that subtropical moisture plumes, which are typically tied to the location of rather stationary anticyclones, can serve as moisture suppliers during the early formation of a cyclone. However, since the cyclone propagation speed typically exceeds that of the lower tropospheric flow by which the moisture is advected (Coronel et al. 2015; Tamarin and Kaspi 2016), they are unlikely to continuously deliver moisture throughout an entire cyclone life cycle. This in turn indicates that midlatitude moisture sources might be most important for the moisture input to cyclones, in particular, beyond their initial intensification phase. Support for this hypothesis is found in the climatological analysis of the origin of moisture in warm conveyor belt inflows, which emphasizes the warm ocean currents as an important source region more so than the subtropics. This holds in particular in winter when cyclones are most intense, whereas in summer also long-range transport from the tropics into ascending warm conveyor belts was found (Pfahl et al. 2014).

Intense ocean evaporation at midlatitudes, and in particular along warm ocean currents, is closely linked to the passage of cyclones via the advection of polar cold air and dry descending air behind the cold front (Zolina and Gulev 2003; Rudeva and Gulev 2011; Papritz et al. 2015; Vannière et al. 2017; Raveh-Rubin 2017; Aemisegger and Papritz 2018), amplified by strong winds, e.g., along the bent-back front and in the cyclone–anticyclone interaction zone (Tilinina et al. 2018). The importance of cyclone-induced marine cold-air outbreaks for the midlatitude moisture budget is underlined by a modeling case study of an intense cold-air outbreak in the Nordic seas. Papritz and Sodemann (2018) estimated that 7% of the total atmospheric water content poleward of 40°N was injected into the atmosphere by ocean evaporation during this single cold-air outbreak. Furthermore, using stable water isotope signals in precipitation, Aemisegger (2018) showed that precipitation in Reykjavík (Iceland), which is predominantly linked to cyclones (Hawcroft et al. 2012), is to a large extent due to water vapor picked up by cold-air outbreaks from the Labrador Sea that form in the wake of cyclones traveling south of Greenland into the Irminger Sea. This suggests that an important fraction of moisture that precipitates in cyclones in fact has its origin in the cold sectors of previously developing cyclones. From a dynamical point of view it is clear, however, that the moisture evaporating into the atmosphere behind the cold front cannot feed into the ascending airstream in the warm sector of that same cyclone, which indicates a potential hand-over of moisture between cyclones.

It is interesting to link those findings with recent studies on cyclone-relative flows. The northeastward propagation of cyclones implies that the system-relative flow is from the east or northeast, feeding air via the so-called feeder airstream from the precyclone environment into the warm sector and, in particular, the inflow region of the warm conveyor belt (Browning and Roberts 1994; Dacre et al. 2019). Numerical sensitivity experiments indeed suggest that the preconditioning ahead of cyclones by surface sensible heat fluxes and ocean evaporation can be an important prerequisite for rapid cyclone intensification (Nuss 1989; Kuo and Low-Nam 1991; Davis et al. 1996; Carrera et al. 1999; Gyakum and Danielson 2000; Bui and Spengler 2021). Furthermore, idealized baroclinic wave experiments indicate that surface evaporation in the precyclone environment provides the bulk of moisture feeding into the warm conveyor belt (Boutle et al. 2010). Finally, Sodemann and Stohl (2013) demonstrated in a case study and with the aid of a mesoscale model equipped with water vapor tracers that in a sequence of frontal-wave cyclones in the North Atlantic, moisture ''left behind'' by one cyclone contributed substantially to precipitation in a subsequent cyclone. Thus, the feeder airstream might provide a pathway for moisture that evaporated in the cold sector of a preceding cyclone or in the cyclone–anticyclone interaction zone to enter the ascent regions of a subsequent cyclone.

Building on these insights, this study is guided by the following specific questions concerning the water cycle related to deep North Atlantic cyclones in winter:

- Q1: For precipitation in the cyclone center, what is the moisture transport distance and for how long does the moisture reside in the atmosphere?
- Q2: What are the geographical and cyclone-relative origins of moisture?
- Q3: In which dynamical environment do moisture uptakes take place; i.e., what is the role of evaporation in the cold sector of preceding cyclones?
- Q4: How do the uptake and moisture transport characteristics change throughout the life cycle of a cyclone?

We will address these questions for a set of 676 cyclones using a state-of-the-art reanalysis dataset and with the aid of a Lagrangian moisture source diagnostic (Sodemann et al. 2008). Limiting the analysis to particularly deep cyclones is motivated by the fact that the deepest cyclones are associated with the most intense precipitation (e.g., Field and Wood 2007; Rudeva and Gulev 2011; Pfahl and Sprenger 2016) and these cyclones also tend to be longer lived, making them more amenable for a life cycle analysis. The geographical focus on the North Atlantic storm track is justified by two arguments. First, many studies addressing the role of air–sea interaction processes for the (rapid) intensification of cyclones and their moisture budget were concerned with cyclones in this basin and the Gulf Stream region. Thus, focusing on North Atlantic cyclones

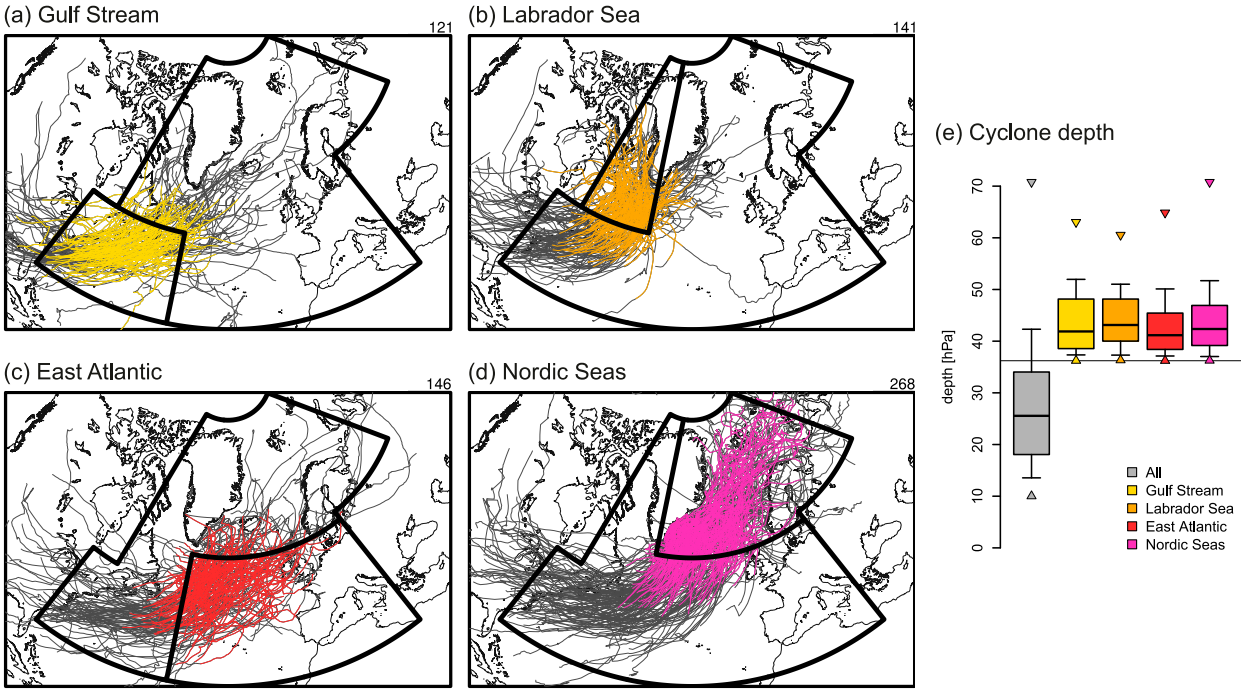

FIG. 1. Tracks of cyclones attaining maximum depth in (a) the Gulf Stream region, (b) the Labrador Sea, (c) the east Atlantic, and (d) the Nordic seas. The tracks' sections between $t = -24$ h before and $t = 24$ h after reaching maximum depth are highlighted in color. Numbers of cyclone tracks are given in the top right of each panel. (e) Distribution of maximum depth of cyclones for the climatology (gray) and selected cyclones in the four subregions (other colors). Whiskers indicate the 10th–90th-percentile range, and triangles show maxima and minima. The black horizontal line indicates the 80th percentile of all tracks, which is used as threshold for the selection of tracks in the four subregions.

facilitates comparison with previous work. Second, limiting the analysis to one ocean basin keeps the discussion about geographical peculiarities focused.

The study is structured as follows. In section 2 we will introduce the dataset, cyclone identification and tracking, as well as the moisture source identification. Then in section 3 we present a detailed case study of a well-studied rapidly intensifying storm over the Gulf Stream [Experiment on Rapidly Intensifying Cyclones over the Atlantic (ERICA) IOP4; e.g., Neiman and Shapiro 1993], followed in section 4 by the climatological analyses of all 676 cyclones. Finally, the paper is concluded by a discussion and final remarks in section 5.

2. Methodology

a. Dataset

The analyses presented in this work are based on the most recent reanalysis dataset ERA5 issued by the European Centre for Medium-Range Weather Forecasts (ECMWF; Hersbach et al. 2020). We use hourly model-level data interpolated on a 0.5° × 0.5° grid for extended winters [November–March (NDJFM)] 1979–2018; that is, November 1979–March 1980 is the first winter and November 2017–March 2018 is the last winter. All fields are analyses except for precipitation and surface evaporation which are short-range forecasts accumulated over one hour intervals.

b. Identification and selection of North Atlantic deep cyclones

We obtain cyclone tracks from hourly sea level pressure (SLP) fields according to the method by Sprenger et al. (2017), which is an improved version of the cyclone identification and tracking scheme introduced by Wernli and Schwierz (2006). At each time step along its track, a cyclone is described by its center defined as the SLP minimum and the outermost closed SLP contour surrounding it, which is obtained from a contour search algorithm with a sampling interval of 0.5 hPa. The pressure difference between the outermost SLP contour and the SLP minimum, the cyclone depth, serves as a measure of cyclone intensity. For each track, we further define a time axis t relative to the time of maximum depth denoted by $t = 0$ h such that $t < 0$ h and $t > 0$ h represent the intensification and decay phase, respectively. In this study, we will determine the moisture sources for precipitation falling in the time interval from $t = -24$ h to $t = 24$ h, which includes the main intensification phase during which more than 50% of the deepening occurs, as well as a substantial part of the decay phase (see online supplemental Fig. 1).

Among all globally identified cyclone tracks in extended winters (NDJFM) 1979–2018, we select a subset of tracks that satisfy the following two criteria: (i) maximum depth is reached in the North Atlantic, including the Labrador Sea, the Nordic seas, and the Barents Sea (cf. Figs. 1a–d), and (ii) tracks extend at least from $t = -24$ h to $t = 24$ h such that each track lasts for

at least 48 h. The second criterion is relatively restrictive as it excludes a number of tracks whose intensification or decay phases are less than 24 h long, which can, for example, happen if the system merges with another cyclone or if it forms as a secondary cyclone. The criterion does, however, ensure that we can consistently investigate the moisture sources and trajectories associated with cyclone precipitation for well-separated stages during the cyclone life cycle, namely, the intensification phase ($t < 0$ h), the mature stage ($t = 0$ h), and the decay phase ($t > 0$ h).

The maximum depth, i.e., the maximum pressure difference between the outermost SLP contour and the SLP minimum attained along a cyclone track, ranges from 10 to more than 70 hPa (Fig. 1e). The distribution is strongly skewed with a long tail toward larger values. Since the focus of this study is on particularly intense cyclones, we restrict the analysis to tracks whose maximum depth exceeds the 80th percentile, yielding a total of 676 tracks. We then divide these remaining tracks further into four groups according to the geographical region where the cyclones attain maximum depth. These regions are the Gulf Stream (121 tracks), the Labrador Sea (141 tracks), the east Atlantic (146 tracks), and the Nordic seas including the Barents Sea (268 tracks). The regions and the corresponding tracks as well as the distributions of the cyclones' maximum depth are shown in Figs. 1a–d and 1e, respectively. Note that a cyclone track can extend outside of the respective region for some time steps in the interval from $t = -24$ h to $t = 24$ h (see colored portion of tracks in Figs. 1a–d).

c. *Moisture source identification*

The identification of moisture sources contributing to precipitation in the cyclone center is based on the computation of kinematic backward trajectories with the Lagrangian Analysis Tool (LAGRANTO; Wernli and Davies 1997; Sprenger and Wernli 2015) and the subsequent application of the moisture source diagnostic by Sodemann et al. (2008) to these trajectories. A similar trajectory-based approach has previously been used for the identification of moisture sources contributing to diabatic potential vorticity changes in cyclones (Čampa 2012). In addition, the moisture source diagnostic has found wide applications, for instance, in the context of heavy precipitation events (Winschall et al. 2014a,b), stable water isotope studies (Aemisegger 2018), and climatological investigations of the global water cycle (Läderach and Sodemann 2016; Sodemann 2020). Winschall et al. (2014a) showed that this trajectory-based method agrees well with computationally more intensive methods using tracers in numerical models, which would not be straight-forward to apply on a climatological basis.

The procedure is schematically outlined in Fig. 2 and follows three main steps:

1) identification of precipitating air parcels near the cyclone center,
2) computation of 8-day kinematic backward trajectories for the previously identified air parcels, and
3) diagnosing moisture uptakes based on the evolution of specific humidity along these trajectories.

These steps are applied along all cyclone tracks in 3-hourly intervals from $t = -24$ h to $t = 24$ h and are detailed in the following.

1) Identification of precipitating air parcels in cyclone center

To identify precipitating air parcels, trajectories are initialized on an equidistant grid with a mesh size of 50 km in the horizontal and 25 hPa in the vertical and from the surface up to a level of 400 hPa. Furthermore, the initialization of trajectories is restricted to a circle with 500-km radius surrounding the cyclone center (see below). Based on a 1-h trajectory computation backward in time, precipitating air parcels are identified by requiring that they (i) are collocated with surface precipitation accumulated over the same hour larger than 0.1 mm h^{-1}, (ii) have cloud water or ice content exceeding 10 mg kg^{-1}, and (iii) experienced a decrease of specific humidity of at least 0.1 g kg^{-1} during the previous hour. The second and third criteria ensure that the air parcels are associated with a cloud and cloud formation occurs at the starting time of the trajectories. All trajectories satisfying these criteria (gray dots in Fig. 2) are then extended to 8 days backward in time, which we found a good compromise between the competing factors of numerical accuracy, computational costs, and the goal to attribute a representative amount of the precipitation to specific sources (cf. section 4a). This results in an average of about 23 000 trajectories per cyclone track, which corresponds to more than 1300 trajectories per initialization time step. As a final step, variables such as specific humidity are traced along the trajectories at 1-h temporal resolution. Despite the fact that trajectories are computed backward in time, we will always consider their evolution forward in time, i.e., the locations in the cyclone core from where backward trajectories are initialized are referred to as the trajectory end points, whereas the trajectory locations 8 days before are referred to as their starting points.

2) Choice of radius around cyclone center

The choice of radius is a compromise between the requirement to include a representative portion of cyclone precipitation and excluding precipitation far from the cyclone center that may be linked to the circulation associated with warm and cold fronts or nearby orography but is likely unrelated to dynamical ascent in the cyclone core. Cyclone-centered composites including all 676 cyclones show that nearly all cyclone- and front-related precipitation falls within 1000 km from the cyclone center (see outer dashed circle in supplemental Fig. 2) except for a band of relatively weak precipitation (<8 mm day^{-1}) to the southwest, likely associated with precipitation falling along trailing cold fronts. Furthermore, the most intense precipitation occurs within less than 500 km (solid circle in supplemental Fig. 2), comprising nearly 50% of all precipitation at $t = -24$ h. Choosing a radius smaller than 500 km, a major portion of precipitation clearly linked to the cyclone core would be omitted, whereas with a larger radius an increasing amount of precipitation linked to fronts or orography would be included. Additional guidance for the choice of radius is obtained from considering precipitation averaged in

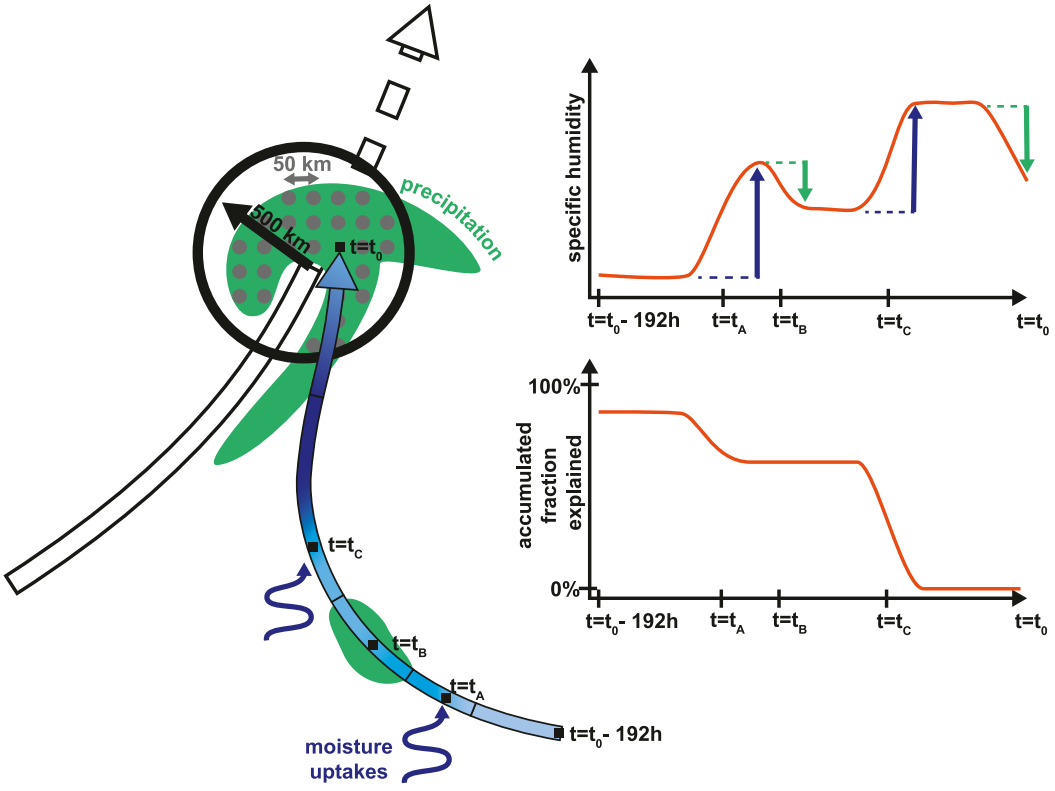

FIG. 2. (left) Schematic illustrating the methodology for detecting moisture sources contributing to precipitation associated with a cyclone. The cyclone track prior to and after precipitation at time $t = t_0$ is shown by the solid and dashed black and white arrow. Green patches indicate where precipitation occurs and the circle with 500-km radius surrounding the cyclone center at $t = t_0$ defines the region in which precipitating air parcels are detected. These air parcels then serve as starting points (gray dots) for the computation of backward trajectories. An example trajectory is colored according to specific humidity with low and high values in light and dark blue, respectively. Moisture uptakes take place at times $t = t_A$ and $t = t_C$, and an intermittent precipitation event along the trajectory occurs at time $t = t_B$. (right) Diagrams showing (top) evolution of specific humidity with moisture uptakes and losses due to precipitation indicated by blue and green arrows, respectively, and (bottom) accumulated fraction of moisture explained by uptakes in the interval between a given time t and t_0. In this particular example, the uptake at $t = t_C$ explains about 60% and the earlier uptake at $t = t_A$ an additional 30% of moisture present at $t = t_0$, leading to an explained fraction of 90% when all uptakes until $t = -192$ h are considered.

circles with radii ranging from 50 to 1000 km (supplemental Fig. 3a), showing a sharp increase of average precipitation up to a radius of 200–300 km and a rapid decrease for larger radii. For radii beyond 500 km, the change in area averaged precipitation with increasing radius starts to converge toward zero (supplemental Fig. 3b), indicating that more and more of the additionally captured precipitation is indistinguishable from a spatially uniform distribution of precipitation and, therefore, can be regarded as unrelated to the cyclone.

3) MOISTURE SOURCE DIAGNOSTICS

Here, we will briefly explain the rationale behind the moisture source diagnostic, while we refer to Sodemann et al. (2008) for a detailed explanation of the methodology. Moisture uptakes are identified as hourly increases of specific humidity along the trajectories exceeding 0.025 g kg^{-1} h^{-1}. This threshold is imposed in order to exclude spurious fluctuations of specific humidity, for instance, due to inaccuracies of the trajectory calculation, and to limit the computational costs of the moisture source diagnostic. Sensitivity experiments revealed that its precise choice has only a weak influence on the fraction of precipitation explained by the identified moisture sources. If intermittent precipitation occurs along a trajectory, identified by a decrease of specific humidity prior to reaching the end point, all uptakes that occurred before the precipitation event are proportionally discounted for by the amount of specific humidity reduction. This is done iteratively starting from $t - 192$ h going forward in time. In contrast to Sodemann et al. (2008), no distinction between uptakes in the boundary layer and above the boundary layer is made. This allows for the possibility that an air parcel can gain moisture via the subgrid-scale convective ventilation of the boundary layer, which may be of particular importance in the convectively unstable cold sectors of cyclones. All so-identified uptakes are finally weighted by the reduction of specific humidity between $t - 1$ h

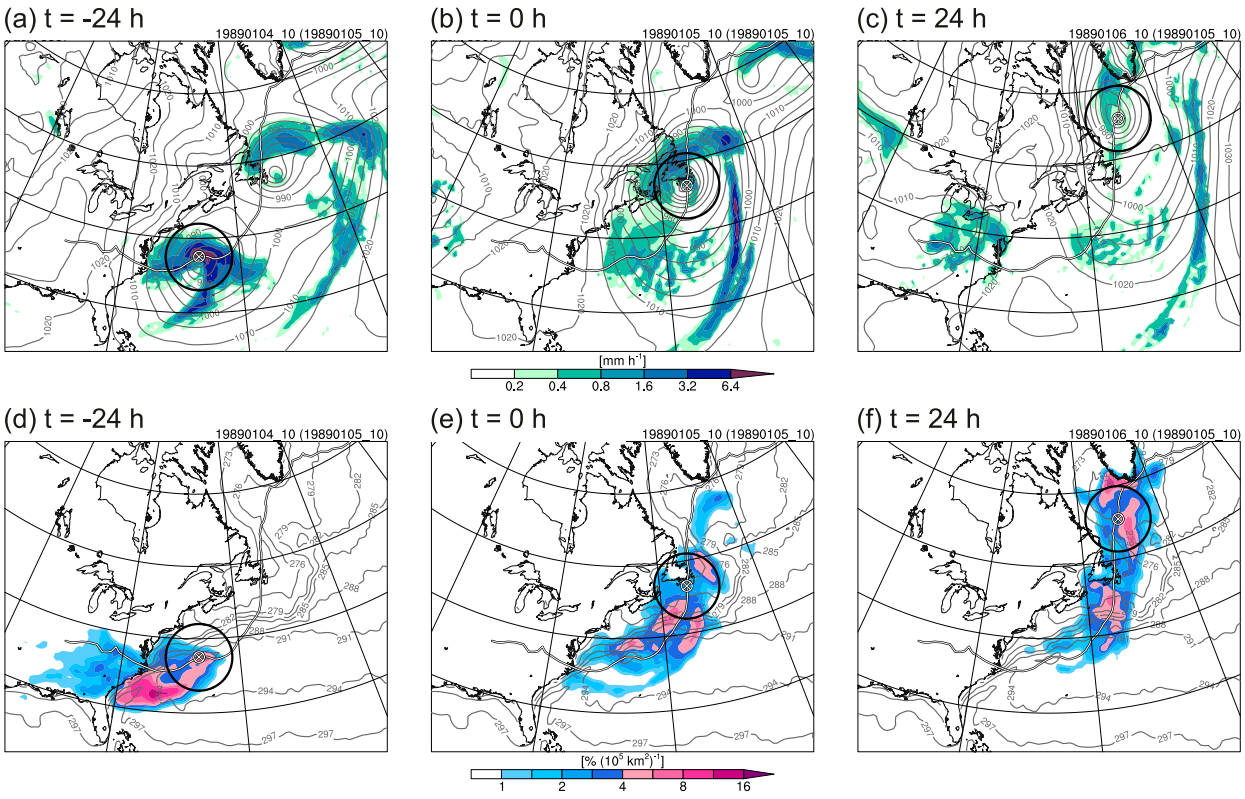

FIG. 3. (a)–(c) Precipitation and (d)–(f) footprints of moisture uptakes contributing to precipitation associated with the ERICA IOP4 storm at (a), (d) $t = -24$ h (1000 UTC 4 Jan 1989), (b), (e) $t = 0$ h (1000 UTC 5 Jan 1989), and (c), (f) $t = 24$ h (1000 UTC 6 Jan 1989). Additionally shown are (a)–(c) SLP (in intervals of 5 hPa; gray contours) and (d)–(f) sea surface temperature (in intervals of 3 K; gray contours), as well as cyclone track (white line) and cyclone center (white cross), and a circle with a radius of 500 km surrounding the cyclone center at the time of precipitation (black circle).

and t yielding the uptakes that contribute to precipitation at the trajectory end point.

The procedure is illustrated for a trajectory in Fig. 2, which experiences two moisture uptakes of approximately the same amount at t_A and t_C, as well as an intermittent precipitation event at t_B. The uptake at t_C fully contributes to the final specific humidity since no precipitation occurs between t_C and t_0. Accordingly, this uptake explains roughly 60% of the final precipitation. The further we go back in time, the more of the precipitation is explained. However, the relative importance of the earlier uptake at t_A is lower than that of the uptake at t_C, even though the increase of specific humidity during both events is the same. The reason for this is the loss of moisture during the precipitation event at t_B. The uptake at t_A must be discounted for proportionally to the amount of moisture lost at t_B such that the uptake at t_A contributes only about 30% to precipitation at t_0. Taking both uptakes into account, about 90% of the precipitation at t_0 is "explained"; i.e., for 90% of the precipitating water, its evaporative source could be identified.

3. Case study of rapidly intensifying cyclone over the Gulf Stream

We begin our analyses with a case study of the ERICA IOP4 storm, a rapidly intensifying marine cyclone that developed in the period 4–5 October 1989 in the western North Atlantic and ranks tenth in terms of depth among the Gulf Stream cyclones considered in this study. Its dynamical evolution has been extensively studied in the context of ERICA (e.g., Neiman and Shapiro 1993). This case study will allow us to anticipate key characteristics of moisture origin and transport into the center of a cyclone that will subsequently be generalized with climatological analyses involving the complete set of deep North Atlantic cyclones in winter.

a. *Moisture sources and transport pathways*

Figure 3 shows precipitation (upper row) associated with the ERICA IOP4 storm from 24 h prior to 24 h after reaching maximum depth as well as the corresponding sources of moisture (lower row) as identified by the moisture source diagnostics. The most intense precipitation in the cyclone center falls during the intensification phase of the cyclone and declines substantially as the cyclone reaches maximum depth and starts to decay (Figs. 3a–c). Corresponding moisture sources are mostly located slightly upstream of the precipitation region throughout the entire cyclone life cycle. Specifically, for precipitation at $t = -24$ h, the sources are located less than 1500 km away from the precipitation region, predominantly on the warm side of the Gulf Stream Front, whereas contributions

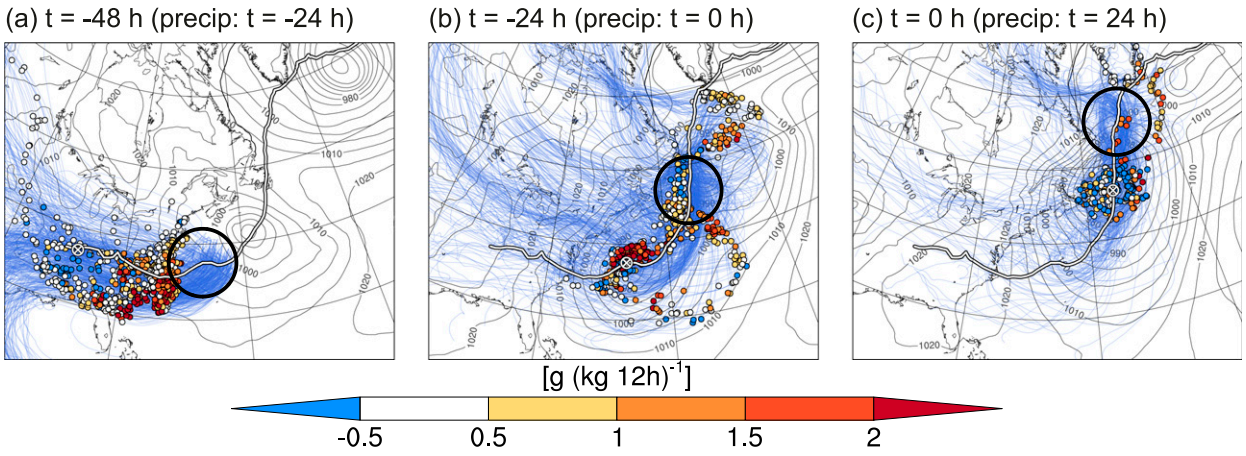

FIG. 4. Trajectories associated with cyclone precipitation at (a) $t = -24$ h (1000 UTC 4 Jan 1989), (b) $t = 0$ h (1000 UTC 5 Jan 1989), and (c) $t = 24$ h (1000 UTC 6 Jan 1989). Further shown are 12-hourly changes of specific humidity along trajectories (colored dots), SLP (in intervals of 5 hPa; gray contours), and the cyclone center (white cross) 24 h before precipitation [i.e., at 1000 UTC 3 Jan 1989 in (a)]. The white line indicates the cyclone track and the black circle shows the 500-km region surrounding the cyclone center from where trajectories are initialized. Note that only every fourth trajectory is drawn.

from land are small (Fig. 3d). Hence, the transport distance of moisture is clearly less than the distance traveled by the cyclone in the same time interval. As the cyclone reaches maximum depth while approaching Newfoundland, the sources of moisture progressively move northward with the cyclone, while the bulk still originates on the warm side of the Gulf Stream Front (Fig. 3e). However, also the colder waters in the vicinity of the precipitation region have notable contributions. This becomes more pronounced for precipitation at $t = 24$ h when most of the water vapor evaporates from a cold ocean surface south of Newfoundland and in the Labrador Sea (Fig. 3f). It is important to note that the amount of precipitation falling at this time is considerably smaller than during the intensification phase of the cyclone.

What are the history and evolution of trajectories linking the moisture source regions and precipitation in the cyclone center? We first consider trajectories associated with precipitation during the intensification phase of the cyclone at $t = -24$ h. Trajectories (Fig. 4a) show that they have previously traversed the United States, some of them following a west–east pathway and others originating from the Gulf of Mexico. The storm has genesis over the eastern United States about 2 days prior to reaching its maximum depth. At that time, most of the trajectories are already located east of the cyclone center off the U.S. East Coast and in close proximity to the target area (indicated by a black circle), where they gain substantial amounts of moisture as evident from the strong increase of specific humidity. This is in line with the overall large contributions of the warm waters associated with the Gulf Stream to the total moisture sources (Fig. 3d). Relatively weak winds lead to a slow transport of the moisture away from the source region. As the storm subsequently propagates toward this region, it catches up with these trajectories and ingests them into the warm sector.

Most of the trajectories linked to precipitation at the time of maximum depth, $t = 0$ h, still come from the North American continent and gain moisture as they traverse the Gulf Stream Front (Fig. 4b). In contrast to trajectories associated with precipitation at $t = -24$ h, however, many trajectories are already located in the vicinity of the intensifying cyclone one day prior to precipitation. In addition, some of the trajectories also originate at higher latitudes and are scattered across a relatively large area northeast of the cyclone center at $t = -24$ h. In particular, a group of trajectories is located in the Labrador Sea and south of Greenland, where they gain moisture over the relatively cold waters (see also Fig. 3e) and subsequently move southward toward the precipitation area.

Finally, trajectories associated with precipitation during the decay phase at $t = 24$ h build two airstreams, a northerly one passing through the Labrador Sea region, eventually flowing southward, and a westerly one with origin over eastern Canada and the northern United States (Fig. 4c). One day prior to precipitation, most of these trajectories are already embedded in the cyclonic flow and some of them show a decrease of specific humidity (blue dots in Fig. 4c) indicating that they contribute to precipitation.

In summary, the trajectories leading to precipitation in the cyclone core reveal a transition from a continuous replenishment of moisture by the flow of humid air into and through the cyclone during its intensification phase, toward a flow configuration where the trajectories recirculate within the more stationary cyclone as it weakens, potentially accompanied by several cycles of moisture uptakes and precipitation within the cyclone.

b. Linkage to synoptic flow evolution

Given that moisture uptakes contributing to precipitation during the cyclone intensification phase take place ahead of the approaching cyclone, the question arises how these uptakes are related to the synoptic flow evolution before the ERICA IOP4 storm enters the stage. In fact, the storm is preceded by a rather dynamic flow evolution dominated by two cyclones, referred to

as C1 and C2, and whose passage across the region is accompanied by a rapid alternation of warm and cold-air advection. Figure 5 depicts daily maps of 900 hPa sea–air potential temperature difference (left column) and instantaneous moisture uptakes (middle column) associated with precipitation in the ERICA IOP4 cyclone any time between $t = -24$ h and $t = 24$ h. The figure further shows water vapor associated with cyclone precipitation (right column), which is obtained from vertically integrating the fraction of the water vapor content of the trajectories that will eventually precipitate in the cyclone.

C1, the first cyclone preceding the ERICA IOP4 storm, is associated with an extensive cold sector characterized by a strongly positive sea–air potential temperature difference (Figs. 5a,d) that reaches at $t = -72$ h (times are still relative to the ERICA IOP4 cyclone) from the Labrador Sea far south of Newfoundland. Such positive sea–air potential temperature differences, i.e., cold air over a warm ocean surface, are accompanied by strong upward fluxes of sensible and latent heat (e.g., Papritz et al. 2015). Notable moisture uptakes eventually contributing to precipitation associated with the ERICA IOP4 storm occur in the southern portions of C1's cold sector and north of the subsequently developing cyclone, C2 (Figs. 5b,e). This confirms that evaporation into the cold sector of a cyclone can eventually feed a subsequent cyclone with moisture.

The moistened trajectories are subsequently advected southward with the cyclonic flow associated with C2 (Figs. 5c,f). Overall the most intense moisture uptakes occur northeast of Florida (Fig. 5h). These uptakes are linked to strong ocean evaporation as relatively warm air is advected off the continent over a very warm ocean surface (see also Figs. 4, 5g). Together with the southward flowing air from further north this leads to an accumulation of moisture off the U.S. East Coast (Fig. 5i). Relatively weak winds keep the moisture in place, allowing the cyclone to catch up during the subsequent 24 h and ingest the humid air into its warm sector (Fig. 5m). Intense moisture uptakes continue to occur throughout the rapid intensification period. They are most prominent in the cyclone's warm sector as well as ahead along the track of the cyclone and the cold sector of C2 (Figs. 5k,l), again underlining the importance of preconditioning of the air masses ahead of a cyclone's track.

c. Summary of key characteristics of moisture uptakes

In light of the questions Q1–Q4 posed at the end of the introduction, the detailed case study of the ERICA IOP4 storm leads us to the following insights:

1) Moisture sources are mainly located in the vicinity of the cyclone track and moisture is transported over short distances compared to the distance traveled by the cyclone itself.
2) Sources of moisture are generally located upstream of the cyclone at the time of precipitation but—at least during its intensification phase—ahead of the approaching cyclone.
3) Surface evaporation in the cold sectors of preceding cyclones is an important source of moisture for precipitation in the subsequent cyclone.
4) The intensification and decay phases are associated with different moisture uptake regions and moisture transport pathways.

In the next section we will investigate to what extent these findings can be generalized for all North Atlantic deep cyclones.

4. Climatology

In this section we consider all selected 676 North Atlantic cyclones and start with a characterization of the moisture uptake conditions, followed by an analysis of the geographical and cyclone-relative uptake locations and transport pathways.

a. Residence time and uptake characteristics

Figure 6 shows the accumulated fraction and daily increase of moisture associated with cyclone precipitation explained by the moisture source diagnostic and as a function of time before precipitation. The identified uptakes along the 8-day backward trajectories explain in total about 90% of precipitating waters at all times of the cyclone life cycle (Fig. 6a). However, most of the uptakes occur within a short time interval before precipitation and moisture uptakes taking place less than 2 days prior to precipitation explain more than 50% of the precipitation. In addition, the largest daily increase of the explained fraction occurs 18 h prior to precipitation with 35%–40% day^{-1} and drops rapidly to less than 5% day^{-1} 5 days prior to precipitation (Fig. 6b). It is interesting to separately consider the uptakes for precipitation falling in the cyclone center associated with the warm conveyor belt. For that purpose, we select the subset of trajectories ascending by at least 600 hPa within 48 h (cf. Madonna et al. 2014). They amount to about 15%–35% of all precipitating trajectories during the intensification phase ($t = -24$ h to $t = 0$ h; Fig. 7d). This reveals that the uptakes associated with the warm conveyor belt occur slightly earlier and over a longer time period than for the average trajectory (Fig. 6a) with a peak of the daily uptake contributions around 36 h prior to precipitation (Fig. 6b). These values are in close agreement with those found by Pfahl et al. (2014), who considered precipitation along the entire warm conveyor belts in the North Pacific, i.e., not only the part close to the cyclone center. The overall large uptake contributions during a short time period prior to precipitation result in a low mean residence time of moisture associated with cyclone precipitation of only approximately 3 days (77, 72, and 71 h for precipitation at $t = -24$ h, $t = 0$ h, and $t = 24$ h, respectively).

Next we characterize the environment in which the uptakes take place and consider how these characteristics change throughout the cyclone life cycle (Figs. 7a,b). More than 50% of the moisture evaporates from a sea surface warmer than 290 K, which is consistent with a moisture origin on the warm side of the Gulf Stream Front. Land contributions remain low around 15% throughout the cyclone life cycle. Already during the intensification phase ($t = -24$ h), more than 50% of the uptakes occur in cold-air outbreak conditions, that is, cold air over a warmer ocean surface as indicated by the positive sea–air potential temperature difference ($\theta_{SST} - \theta_{900} > 0$ K; Fig. 7a). About half of these uptakes are associated with convectively highly unstable conditions in relatively strong cold-air outbreaks ($\theta_{SST} - \theta_{900} > 4$ K) that are accompanied by

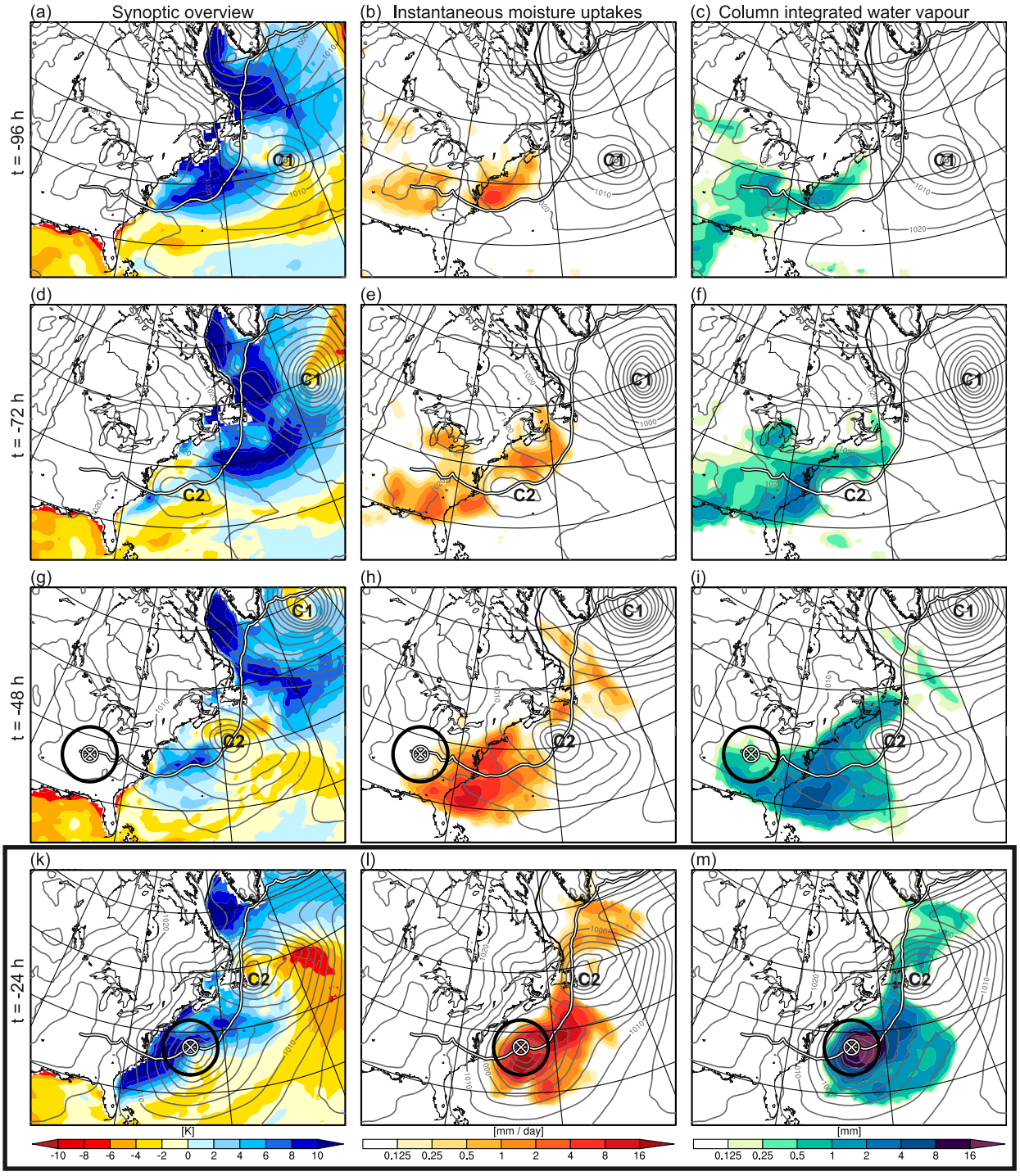

FIG. 5. Evolution of the ERICA IOP4 storm over the Gulf Stream for (a)–(c) $t = -96$ h (1000 UTC 1 Jan 1989), (d)–(f) $t = -72$ h (1000 UTC 2 Jan 1989), (g)–(i) $t = -48$ h (1000 UTC 3 Jan 1989), and (k)–(m) $t = -24$ h (1000 UTC 4 Jan 1989). Shown are (left) sea–air potential temperature difference ($\theta_{SST} - \theta_{900}$), as well as (center) instantaneous moisture uptakes and (right) vertically integrated water vapor associated with cyclone precipitation in the time interval $t = -24$ h to $t = 24$ h. Note that vertically integrated water vapor comprises only the fraction that eventually precipitates in the cyclone center. Additionally shown are SLP (in intervals of 5 hPa; gray contours), sea ice edge (50% sea ice concentration; thin black contour), cyclone track (white line), cyclone center (white cross), and surrounding circle with a radius of 500 km (black circle). Labels C1 and C2 denote two cyclones preceding the ERICA IOP4 storm. Note the logarithmic color scales for instantaneous moisture uptakes and vertically integrated water vapor.

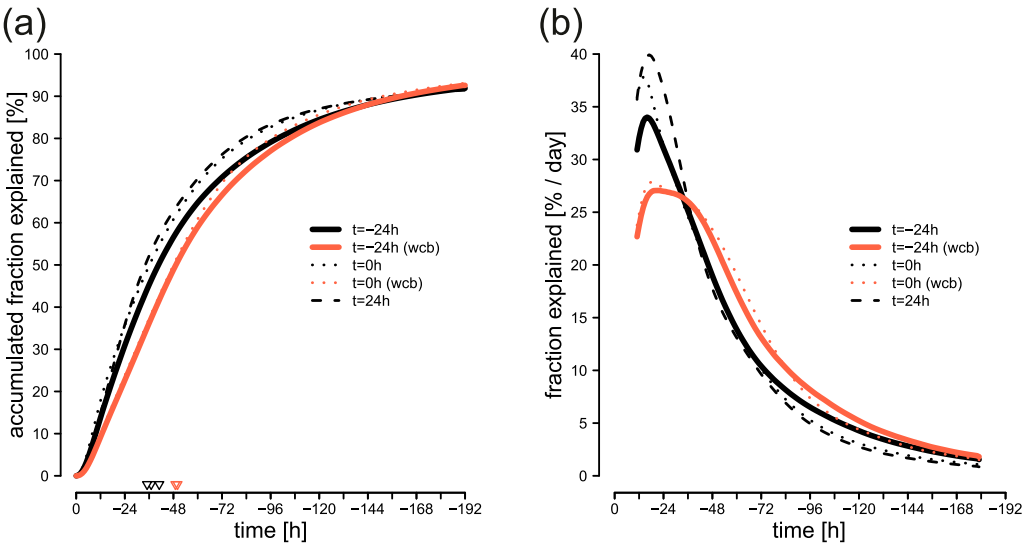

FIG. 6. (a) Accumulated fraction of explained precipitation and (b) contributions of uptakes per day as a function of time for precipitation at $t = -24$ h (solid), $t = 0$ h (dotted), and $t = 24$ h (dashed) for all trajectories (black) and warm conveyor belt (WCB) trajectories (red). Triangles in (a) indicate the time at which the accumulated fraction reaches 50%. Note that the time axis is relative to the time of precipitation and cyclones from all regions are included.

intense upward turbulent heat fluxes. An additional 30% of the uptakes occur under convectively stable conditions typical for a cyclone's warm sector with warmer air than the underlying ocean surface and downward sensible heat fluxes.

When the cyclones reach peak intensity and thereafter ($t \geq 0$ h), contributions from colder waters increase markedly (Fig. 7b). At the same time, also the uptakes in cold-air outbreak conditions rise to 65% by $t = 24$ h at the expense of contributions in warm sector conditions (Fig. 7a). These shifts reveal that—as the cyclone matures—cyclone precipitation is not primarily linked to poleward transport of moisture from southerly origins, for example, within the cyclone or along its cold front. Instead, they indicate that the cyclones propagate into an environment that has previously been moistened in the context of cold-air advection. This view receives further support by the overall small transport distance of moisture between uptake and precipitation (Fig. 7c). Already, at $t = -24$ h more than 50% of moisture is transported by less than 1500 km and less than 15% originates more than 3000 km away. At $t = 24$ h the fraction of moisture originating less than 1500 km away increases even to 70% and less than 10% of the moisture is transported by more than 3000 km.

In line with the case study of the ERICA IOP4 storm, these findings lend support to the hypothesis that moisture uptakes in the cold sectors of cyclones play an important role for supplying subsequent cyclones with moisture. The goals of our following analyses are twofold. First, we aim to pinpoint the geographical origin of the moisture and link it, in particular, to the Gulf Stream Front. Second, we will consider the moisture source locations in a cyclone-relative frame of reference to further our understanding of the role of preceding cyclones' cold sectors in preconditioning the environment into which cyclones propagate.

b. Geographical origin of moisture

In this section we analyze the geographical distribution of moisture uptakes. Figure 8 shows separate moisture source footprints for cyclones reaching maximum intensity in one of the four subregions (rows) and for precipitation at representative times during the intensification phase ($t = -24$ h), the mature stage ($t = 0$ h), and the decay phase ($t = 24$ h).

The distribution of moisture sources associated with cyclone precipitation during the intensification phase ($t = -24$ h) is surprisingly similar for the cyclones in all subregions. Consistent with the cyclone location at the time of precipitation (red crosses) combined with the previously identified short residence time of moisture and the small travel distance, moisture uptakes are restricted to the western North Atlantic and are concentrated on the warm side of the Gulf Stream Front and its extension—the kink in sea surface temperature east of Newfoundland (Figs. 8a,d,g,k). Contributions from more remote locations such as the subtropics, land, or cold waters remain small in agreement with the previous analyses. The moisture source footprints of cyclones in the east Atlantic and the Nordic seas are shifted northeastward toward the Gulf Stream Extension (Figs. 8g,k) as compared to cyclones in the Gulf Stream and the Labrador Sea regions (Figs. 8a,d). In addition, Gulf Stream cyclones also receive an important fraction of their moisture from the Gulf of Mexico (Fig. 8a).

For precipitation at the mature stage ($t = 0$ h), moisture uptake regions for Gulf Stream cyclones remain nearly identical to those during the intensification phase (Fig. 8b), whereas for cyclones in the other regions they shift away from the Gulf

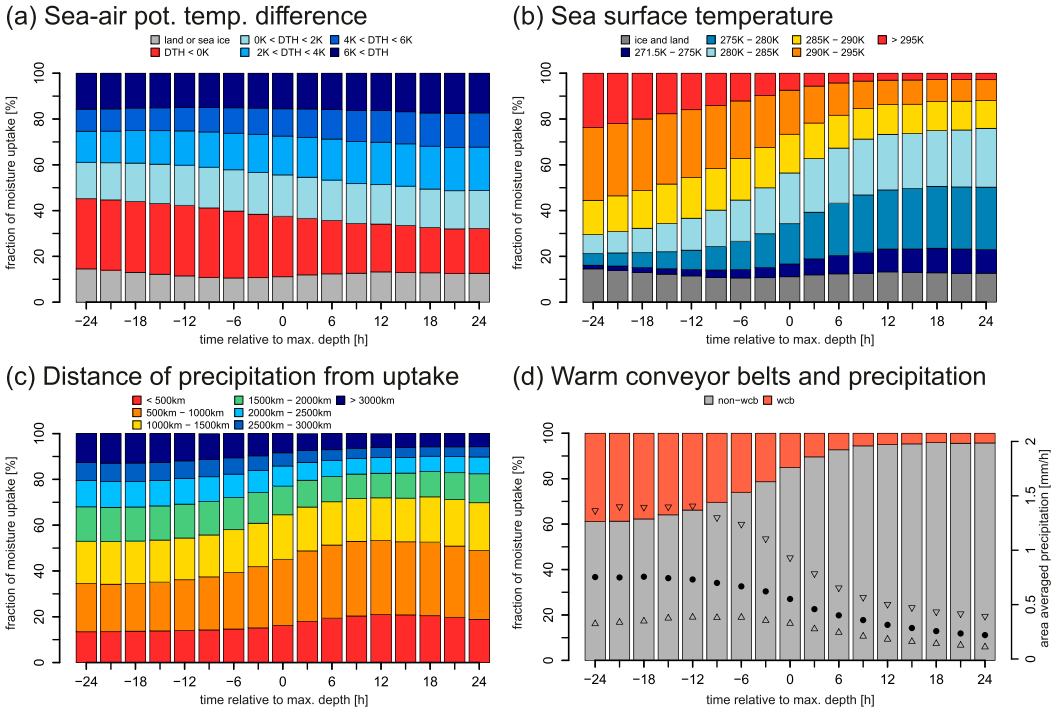

FIG. 7. Characteristics of moisture uptakes contributing to precipitation at $t = -24$ h to $t = 24$ h in 3-hourly intervals associated with cyclones from all regions. Shown are uptake contributions according to (a) sea–air potential difference $\mathrm{DTH} = \theta_{\mathrm{SST}} - \theta$ and contribution from land and ice, (b) sea surface temperature, (c) great circle distance between uptake and precipitation locations, and (d) fraction of uptakes associated with precipitation along trajectories satisfying the warm conveyor belt criterion [i.e., ascent > 600 hPa $(48\,\mathrm{h})^{-1}$], as well as cyclone precipitation (averaged over circles with 500-km radius around cyclone centers) with dots and triangles indicating median and 10th and 90th percentiles, respectively.

Stream Front toward the colder waters along the cyclone tracks (Figs. 8e,h,l). Furthermore, for precipitation during the decay phase of cyclones ($t = 24$ h) moisture uptakes in the marginal seas of the North Atlantic such as the Labrador Sea, the Irminger Sea, and the Nordic seas become dominant (Figs. 8f,i,m) except for Gulf Stream cyclones for which both the Gulf Stream Front and the Labrador Sea are important (Fig. 8c).

Comparing moisture uptakes with mean cyclone tracks (white lines) and cyclone positions at the time of precipitation (crosses) suggests that uptakes contributing to precipitation during the intensification phase tend to be located along the cyclone tracks and upstream of where the precipitation falls. During the decay phase, in contrast, cyclone propagation is slow and for all cyclone groups, except Gulf Stream cyclones, uptakes originate from an area surrounding the cyclone center at the time of precipitation. Thus, these uptakes and related trajectories may be closely linked to the wrap-up of cold air around the cyclone center characteristic of this stage of cyclone development. In the following, we aim to corroborate these hypotheses further by considering the uptake locations in a cyclone-relative perspective.

c. *Cyclone-relative perspective*

To better understand the large-scale environment in which moisture uptakes take place and the moisture pathways from the evaporation regions toward the cyclone, we compile composites in a cyclone-relative frame of reference. For that purpose, we interpolate fields for a given cyclone and relative time t onto a rotated longitude–latitude grid in which the equator and the prime meridian intersect at the center of the cyclone given by the sea level pressure minimum. Note that for simplicity we do not rotate the fields relative to the cyclone propagation direction. Afterward, we average the interpolated fields over all 676 cyclones, yielding the desired composites.

It is instructive to first consider the spatial distribution of instantaneous ocean evaporation in the vicinity of the cyclones and how it changes throughout their evolution (Fig. 9). During the early stages of cyclone development, the composites of SLP reveal a pronounced anticyclone southeast of the developing cyclone and a low northeast (Fig. 9a–c), which in many cases may be a parent low of the intensifying (secondary) cyclone. Two regions with strong ocean evaporation are apparent: the interaction zone of the high and low pressure system (denoted "A" in Fig. 9c) and the area within and south of the anticyclone (denoted "B"). The intensity of evaporation in these two regions gradually declines as time evolves and at the same time evaporation in the cold sector of the intensifying cyclone (denoted "C") becomes the region with the most intense evaporation (Figs. 9d,e), peaking around the time of maximum depth of the cyclone ($t = 0$ h; Fig. 9g) and declining afterward (Figs. 9h,i).

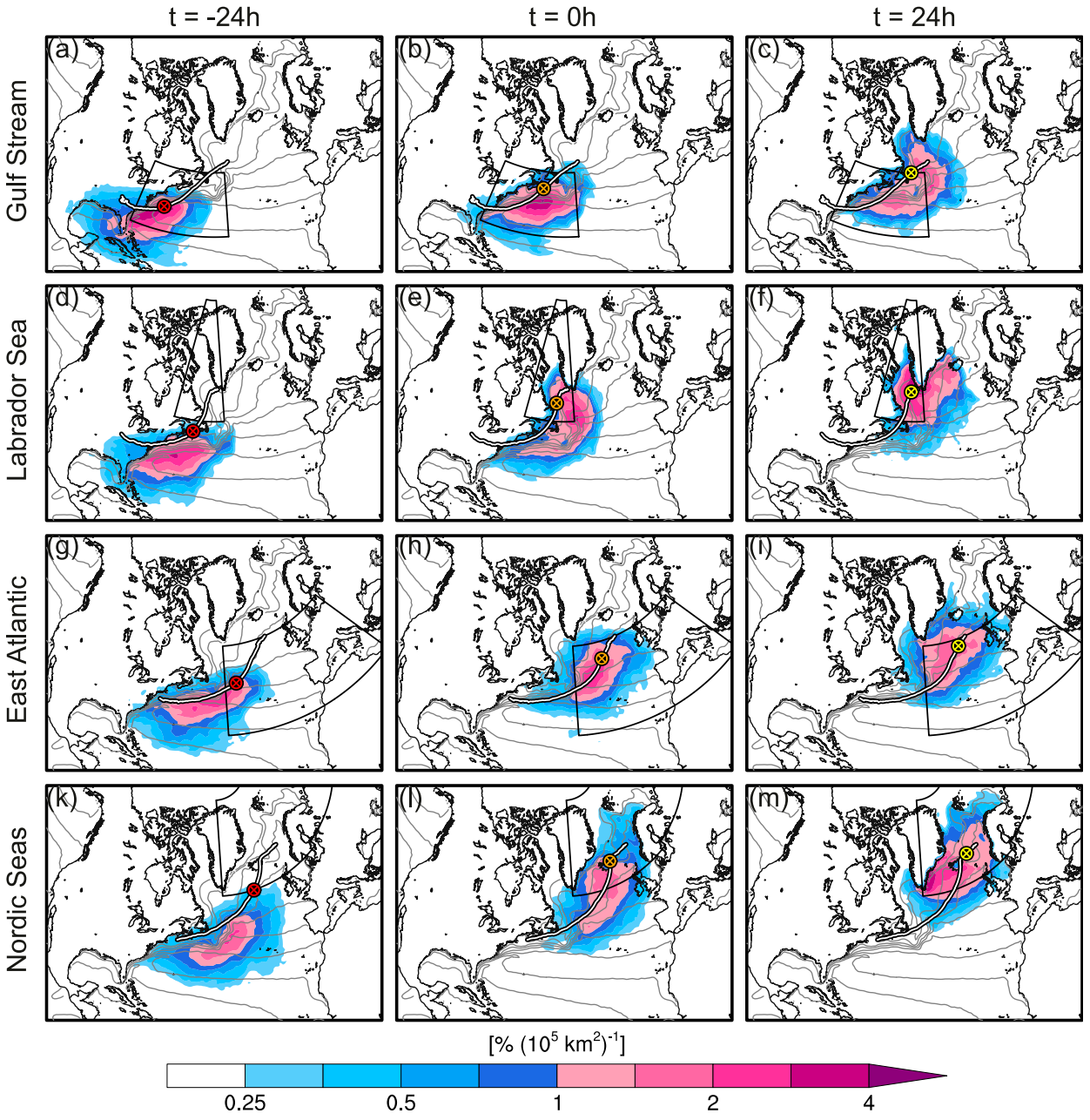

FIG. 8. Climatological footprints of moisture uptakes contributing to precipitation at (a),(d),(g),(k) $t = -24$ h, (b),(e),(h),(l) $t = 0$ h, and (c),(f),(i),(m) $t = 24$ h associated with cyclones in (a)–(c) the Gulf Stream region, (d)–(f) the Labrador Sea, (g)–(i) the east Atlantic, and (k)–(m) the Nordic seas. Gray contours show sea surface temperature in intervals of 3 K and the mean cyclone tracks for $t = -72$ h to $t = 48$ h (white line) as well as the mean cyclone position at the time of precipitation (cross). The regions used for selecting cyclones at their time of maximum depth are outlined by black frames.

The dynamical context of evaporation in the three regions is very different. In A and C, the north-westerly flow–associated in the former with the downstream (parent) low and in the latter with the intensifying cyclone itself—brings cold air over a comparatively warm ocean surface. In addition, wind speeds in the cyclone–anticyclone interaction zone are often very high, contributing to intense upward surface heat fluxes (Tilinina et al. 2018) and carrying the evaporate rapidly downstream. However, there is also a relatively calm region as indicated by the weak pressure gradients slightly west of A (Fig. 9c). The track of the cyclone passes close to this region with the cyclone center at $t = -24$ h effectively located nearby and at $t = 0$ h slightly north (see orange cross in Fig. 9c). The evaporation region B, in contrast, is more remote relative to the cyclone and surface evaporation takes place into rather warm, subsaturated air that subsided in the

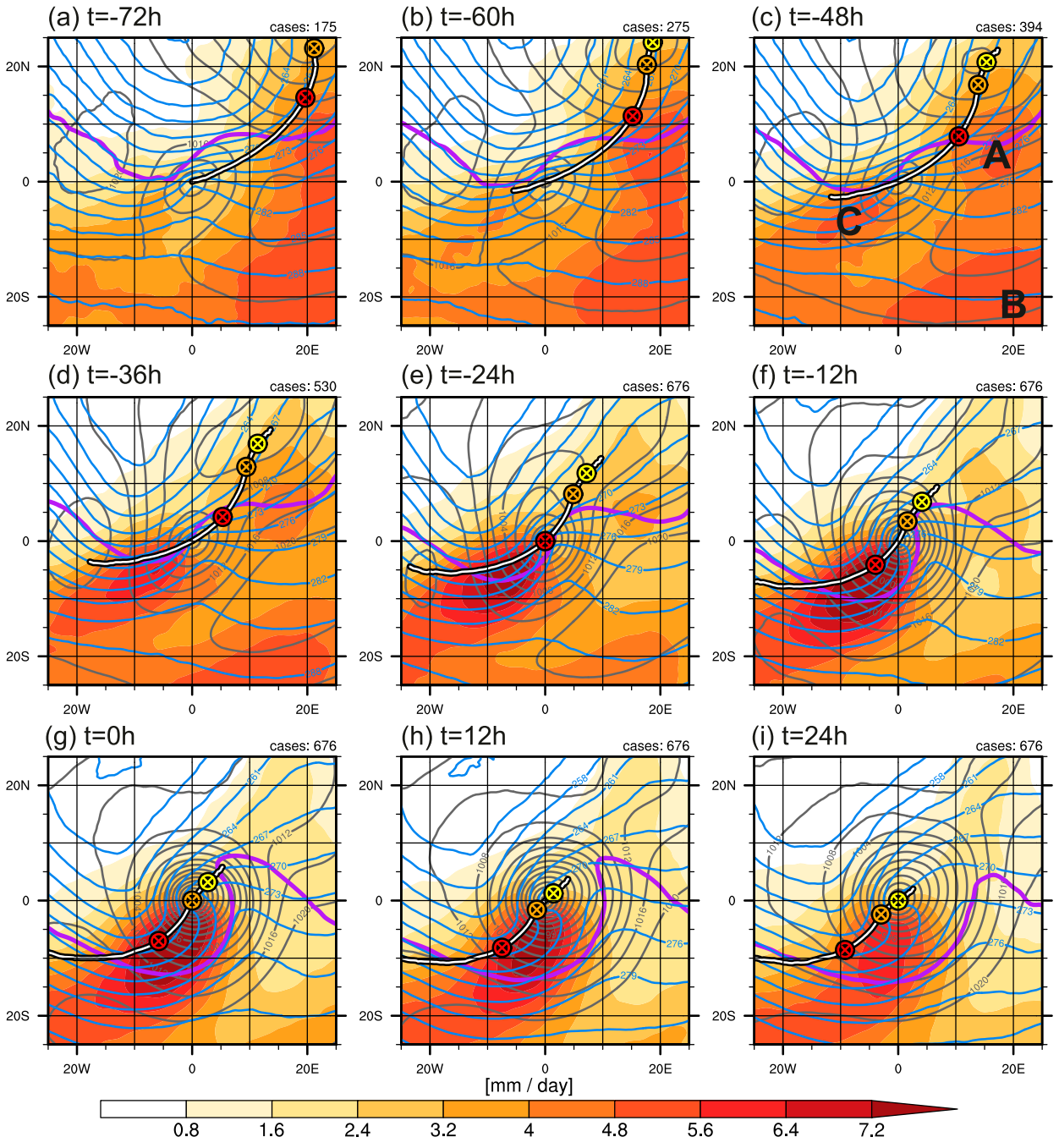

FIG. 9. Cyclone-relative composites for cyclones from all regions showing surface evaporation (shading), potential temperature at 900 hPa (in intervals of 3 K; blue contours), SLP (in intervals of 4 hPa; gray contours), and the 2-PVU contour at 315 K (purple; 1 PVU = 10^{-6} K kg^{-1} m^2 s^{-1}) for $t = -72$ h to $t = 24$ h in 12-hourly intervals. Additionally shown are the mean cyclone track between $t = -72$ h to $t = 48$ h (white line) and cyclone center at $t = -24$ h (red cross), $t = 0$ h (orange cross), and $t = 24$ h (yellow cross). Labels A–C denote the main evaporation regions discussed in the text and the number of cyclones contributing to the composites is indicated in the top right of each panel.

anticyclone. Finally, evaporation in C represents evaporation in the cyclone's own cold sector. Since C is dynamically decoupled from the cyclone's warm sector, it is unlikely to contribute substantially to the precipitation during the intensification phase of the cyclone but may become relevant for precipitation during the decay phase when the cold sector air is wrapped around the cyclone core. From the uptake characteristics found in section 4a, namely, (i) the

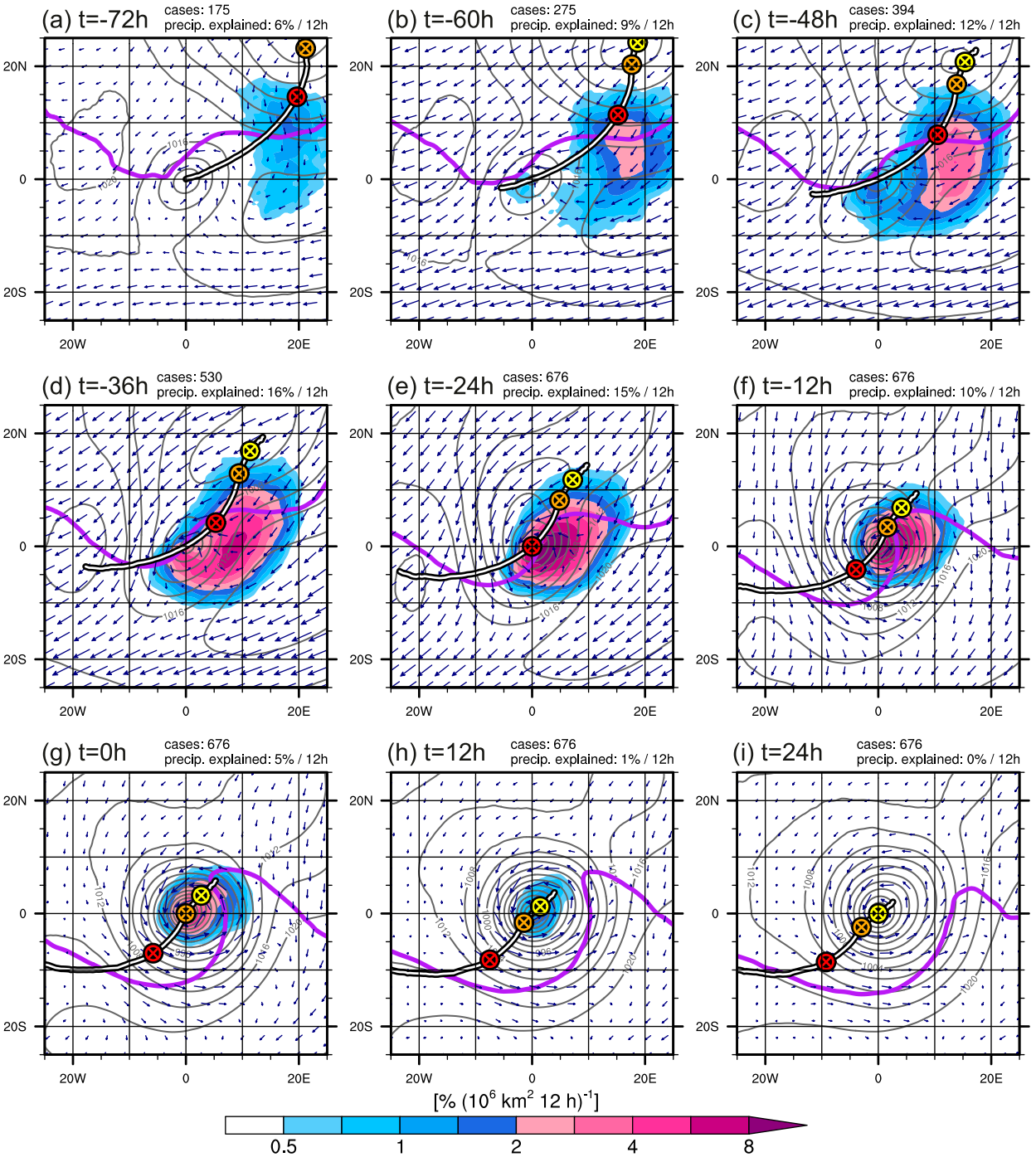

FIG. 10. As in Fig. 9, but for instantaneous moisture uptakes contributing to cyclone precipitation between $t = -24$ h and $t = 24$ h (shading) and cyclone-relative winds at 900 hPa (vectors) defined as the actual 900-hPa winds minus the 12-h average cyclone propagation speed obtained from the cyclone tracks. Furthermore, the number of cyclones contributing to the composites and the percentage of cyclone precipitation explained by the composited uptakes shown in the corresponding panel is indicated in the top right.

short residence time of moisture, (ii) the small transport distances between uptake and precipitation, and (iii) the fact that much of the uptakes occur in cold-air outbreak conditions, we expect A to be the dominant moisture source region.

In Fig. 10 we show cyclone-relative instantaneous moisture uptakes contributing to cyclone precipitation. In contrast to Fig. 9, which showed the entire evaporation field, here we only consider evaporative moisture sources that eventually

contribute to precipitation in the center of the considered cyclones at any time between $t = -24$ h and $t = 24$ h. This figure confirms that moisture uptakes at $t = -48$ h, explaining 27% of the precipitation, occur predominantly in A and in the calm region to the west (Figs. 10a–c). Uptakes between $t = -48$ h and $t = -24$ h explain 31% of the precipitation and the uptake locations gradually shift from A toward the warm sector of the cyclone (Figs. 10d,e). An additional 16% of precipitation is explained by uptakes from $t = -12$ h onward with source locations in close proximity to the cyclone. Furthermore, after $t = 0$ h, most of the uptakes occur predominantly within 500 km from the cyclone center and include the cyclone's cold sector, i.e., evaporation region C (Figs. 10f–i). Note that the remaining 26% of moisture contributing to cyclone precipitation are either unexplained (10%) or they occur before $t = -72$ h (16%; cf. Fig. 6a).

Since the amount of precipitation decreases substantially from the intensification to the decay phase of the cyclone (cf. Fig. 7d), the bulk of the uptakes shown in Figs. 10a–f is linked to precipitation during the intensification phase, masking the importance of uptakes in the cyclone's own cold sector C for precipitation during the decay phase. However, considering only uptakes contributing to precipitation at $t = 24$ h reveals that merely a small fraction of the moisture originates from the precyclone environment (cf. supplemental Figs. 4c,f). Instead, most of the moisture uptakes occur in the vicinity of the cyclone with a maximum in its cold sector, that is, in region C.

d. *Transport pathways and importance of cyclone propagation*

The distribution of moisture uptakes relative to the cyclone confirm the hypothesis stated at the end of the ERICA IOP 4 case study, namely, that evaporation in the cyclone–anticyclone interaction zone ahead and in the cold sector of a preceding cyclone are key for precipitation during the cyclone's intensification phase. This raises the question about the nature of the involved moisture transport and how the moistened air enters the ascent regions of the developing cyclone.

To elucidate this further, we first consider in Fig. 11 the temporal evolution of average vertical profiles of potential temperature and specific humidity along trajectories, as well as the location of the trajectories within these profiles. For that purpose, we select the set of trajectories associated with precipitation at $t = -24$ h and for which daily average moisture uptakes peak between $t = -72$ h and $t = -48$ h (i.e., 48–24 h prior to precipitation). This selection is necessary to obtain meaningful vertical profiles. However, we note that the profiles and their temporal evolution are qualitatively similar for trajectories whose moisture uptakes peak before or after that time interval, as well as for trajectories linked to precipitation at $t = 0$ h (not shown).

Between $t = -120$ and 72 h prior to precipitation, the median pressure of the trajectories is around 750 hPa (Fig. 11a), above a dome of cold air, often part of the cold sector of a parent low as indicated by the low surface pressure values for many of the trajectories (Fig. 11c). Subsequently, the trajectories descend from above this dome of cold air and enter the boundary layer (Fig. 11a, orange contours) as they approach

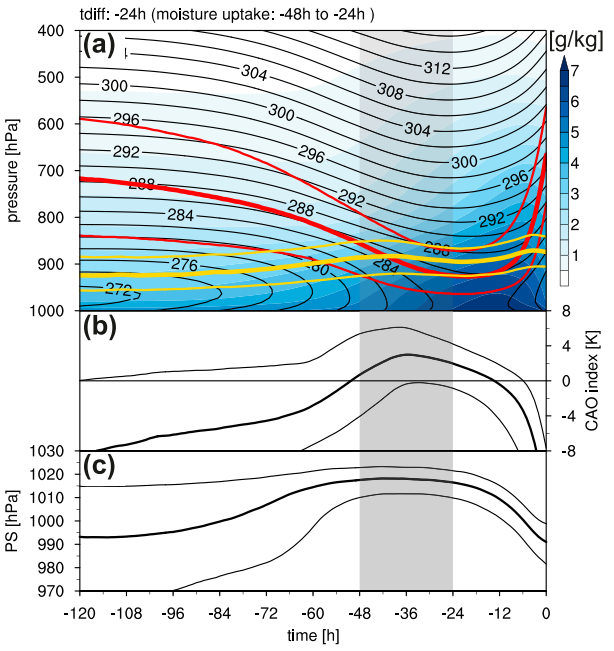

FIG. 11. (a) Lidar cross section along trajectories associated with precipitation at $t = -24$ h with the maximum daily average moisture uptake between 48 and 24 h prior to precipitation as indicated by gray shading. Shown are specific humidity (shading), potential temperature (in intervals of 2 K; black), pressure at trajectory positions (red), and pressure at the top of the planetary boundary (yellow). (b), (c) Evolution along trajectories of (b) sea–air potential temperature difference ($\theta_{SST} - \theta$; CAO index) and (c) surface pressure. Thick contours indicate the median and thin contours the 25th and 75th percentiles. Note that the time axis is relative to the time of precipitation.

the cyclone–anticyclone interaction zone (region A). Despite originating above the dome of cold air, these trajectories tend to be colder than the sea surface [see positive cold-air outbreak (CAO) index in Fig. 11b]. Adiabatic warming due to the descent and diabatic warming by surface sensible heat fluxes both contribute to a pronounced subsaturation of these trajectories, resulting in strong moisture uptakes. The moistened trajectories then approach the developing cyclone within the boundary layer as evident by the decreasing surface pressure (Fig. 11c), followed by rapid, cross-isentropic ascent during the final 12 h.

The trajectories picking up moisture in A are embedded in a weak westerly background flow (low pressure to the north, high pressure to the south; see Fig. 9c)—yet they contribute to precipitation in the center of the developing cyclone located upstream. This result follows from the fact that the cyclone propagates northeastward at a faster speed than the speed of the trajectories, giving rise to a northeasterly cyclone-relative airflow. This is illustrated by cyclone-relative winds at 900 hPa (arrows in Fig. 10), the typical level of the trajectories between evaporation region A and the cyclone warm sector (Fig. 11). Between $t = -60$ h and $t = -24$ h the cyclone-relative flow at 900 hPa is essentially directed southwestward from the moisture uptake regions toward the cyclone and into its warm sector (Figs. 10b–e), corresponding to the feeder airstream

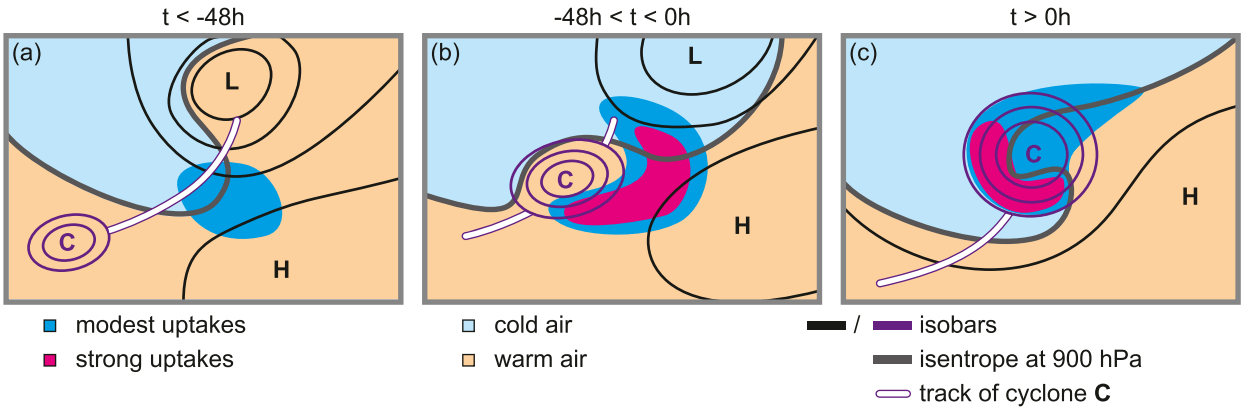

FIG. 12. Schematic summarizing moisture uptakes at (a) $t < -48$ h, (b) $-48 < t < 0$ h, and (c) $t > 0$ h contributing to precipitation associated with cyclone C from a cyclone-relative point of view.

introduced by Dacre et al. (2019). It is interesting to note that the cyclone-relative location of the moisture sources is fairly insensitive to the cyclone propagation speed as long as the propagation direction is toward the northeast (supplemental Figs. 5b–e), which is generally the case for the North Atlantic cyclones considered here (supplemental Fig. 5a). Finally, the mean cyclone track reveals that cyclone propagation becomes much weaker for $t \geq -12$ h. Accordingly, the cyclone-relative flow transforms into a nearly closed cyclonic circulation around the cyclone center, in line with the dominant moisture sources now located in the vicinity of the cyclone center (Figs. 10f–i).

5. Concluding remarks

a. Synthesis

In this study we characterized the water cycle associated with 676 wintertime North Atlantic deep cyclones and pinpointed the moisture sources and uptake conditions of precipitation falling within 500 km from the cyclone center and how they change throughout the cyclone life cycle. For that purpose, we computed a large ensemble of kinematic backward trajectories from precipitating air parcels within a 500-km radius of the cyclone centers and diagnosed the moisture uptakes along the trajectories. Thus, our key findings in light of the questions Q1–Q4 posed in the introduction are as follows:

Q1: The water cycle associated with North Atlantic deep cyclones is characterized by a short transport distance as compared to the distance traveled by the cyclones themselves. Long-range transport from remote sources, such as the subtropics or land areas, is of minor importance at all times of the cyclone evolution. Consistent with the short transport distance, 50% of the uptakes occur less than 2 days prior to precipitation, resulting in a mean residence time of explained precipitation of only about 3 days.

Q2: Geographically, the warm side of the Gulf Stream Front and its northeastward extension—the kink of the SST front east of Newfoundland—are the dominant moisture source regions for all cyclones. Thereby, cyclones reaching maturity in the east Atlantic and the Nordic seas have larger contributions from the Gulf Stream Extension than from the Gulf Stream Front itself. Throughout the cyclone evolution, the moisture sources shift along the cyclone tracks toward the colder waters in the respective ocean basins where the cyclones reach maturity and ultimately decay.

Q3: More than 50% of the uptakes occur in air that is substantially colder than the sea surface as typical for the cold sectors of cyclones. Indeed, cyclone-relative composites revealed that substantial uptakes occur in the cold sector of a preceding low pressure system and in the cyclone–anticyclone interaction zone downstream of the considered cyclone. Uptakes in the cyclone's own cold sector contribute substantially to precipitation during the system's decay when the cold sector air is wrapped around the cyclone's core.

Q4: The dynamical environment of the uptakes is schematically summarized in Fig. 12. It changes profoundly throughout the cyclone life cycle concomitant with the characteristics of the cyclone-relative flow.

- Intensification phase ($t < 0$ h): Uptakes occur ahead and to the east of the cyclone in cold and dry air that descended over a dome of cold sector air into the planetary boundary layer. The cyclone propagation is directed toward this region and as its propagation speed exceeds the advection speed, the moistened air converges at the base of the cyclone's ascent region (Figs. 12a,b).
- Decay phase ($t > 0$ h): As the cyclone starts to decay, the cyclone-relative flow changes from a flow through the cyclone to a confined flow where cold sector air is wrapped up cyclonically around its core. Consequently, precipitating waters originate to a large degree in the cyclone's own cold sector (Fig. 12c).

Our findings reveal that the evaporative moisture source regions for cyclone precipitation are the result of a combination of (i) environmental conditions that favor significant ocean evaporation and (ii) the cyclone propagation that largely influences the direction of the cyclone-relative flow and

determines which air is transported to the base of the ascent regions in the cyclone center.

b. *Discussion and final thoughts*

Favorable conditions for strong ocean evaporation at midlatitudes exist mainly in the cold sectors of cyclones and in the attendant large-scale cold-air outbreaks, as well as cyclone–anticyclone interaction zones with their strong winds. A novelty of our study is the systematic analysis of the thermodynamic and large-scale dynamical environments of moisture uptakes throughout the cyclone life cycle, including, in particular, also the decay phase. In that respect our study complements the analysis of moisture sources contributing to precipitation along warm conveyor belts by Pfahl et al. (2014), while at the same time corroborating the short residence time of moisture and importance of local sources as compared to remote ones. Our results emphasize the importance of moisture uptakes by cold and dry air, which have previously been found to provide the preferred conditions for strong large-scale ocean evaporation at mid- and high latitudes (Aemisegger and Papritz 2018), throughout the entire cyclone life cycle.

Furthermore, our analyses reveal that especially early uptakes, sometimes occurring well before genesis of the cyclone (e.g., ERICA IOP4 case study), are closely linked to the cold sector of a preceding cyclone (Fig. 12a). This is reminiscent of the hand-over of moisture from one cyclone to the next as proposed by Sodemann and Stohl (2013) based on the analysis of a sequence of North Atlantic frontal cyclones. The large set of cyclones analyzed here confirms that this hand-over of moisture is not a peculiarity of their specific case but instead appears to be a general feature of the water cycle along a storm track with consecutive cyclone development.

The feeder airstream—a cyclone-relative flow from the northeast—bringing moist air from the precyclone environment into the warm sector is a key element of water vapor transport in cyclones and in their environment. Its significance for the water budget of cyclones was pointed out previously by Dacre et al. (2019). It provides the mechanistic linkage between the region of strong ocean evaporation ahead of a cyclone, identified in this study as the dominant moisture source region for precipitation falling during cyclone intensification, and the actual precipitation that takes place in the cyclone center. This airstream owes its existence purely to the cyclone propagation. Thermal steering of a developing cyclone, characterized by the continuous generation and destruction of relative vorticity ahead and behind the vorticity maximum, respectively (Sutcliffe 1947; Hoskins and Pedder 1980), as well as diabatic heating in the poleward, ascending flow (Coronel et al. 2015; Tamarin and Kaspi 2016) imply a (north)eastward propagation of a cyclone that exceeds the advection by the background flow in the lower troposphere. Consequently, lower tropospheric air from ahead of the cyclone track continuously enters the cyclone and subsequently flows through it. Combined with the fact that this air tends to be originally cold and dry, this mechanism provides an explanation for the high sensitivity of rapid cyclone intensification to surface fluxes in the precyclone environment (Nuss 1989; Kuo and Low-Nam 1991; Davis et al. 1996; Carrera et al. 1999; Gyakum and Danielson 2000; Giordani and Caniaux 2001; Bui and Spengler 2021).

Our study has interesting implications for the understanding of the processes that set the fundamental characteristics of the atmospheric water cycle at midlatitudes and, in particular, along midlatitude storm tracks. The fact that precipitating waters in the center of a deep cyclone originate to a large degree in the cold sector of a preceding cyclone or their own suggests that a storm track generates—to some extent—its own water cycle whose characteristic spatial and temporal scales are determined by the respective scales of baroclinic waves. More specifically, the life time of water vapor is essentially set by the time between the transit of one cyclone and the next, that is, approximately 2 days. This is in close agreement with the values obtained here (≈3 days) as well as climatological estimates of the water vapor residence time along the North Atlantic storm track (Läderach and Sodemann 2016; Sodemann 2020). Cyclone propagation into the moisture uptake region further implies that the transport distance of moisture is smaller than the distance traveled by the cyclone itself, suggesting that the water cycle along a storm track is spatially more confined than the storm track itself.

Even though cyclones constitute the most important precipitation-generating weather system at midlatitudes, a nonnegligible part of midlatitude precipitation falls outside the centers of deep cyclones in different dynamical settings such as along extended frontal structures (Catto et al. 2012; Catto and Pfahl 2013; Papritz et al. 2014) or associated with atmospheric rivers interacting with potential vorticity streamers or orography (e.g., Ralph et al. 2011; Sodemann et al. 2020; de Vries 2021). While the feeder airstream has been shown to contribute to moisture convergence along cold fronts and the maintenance of atmospheric rivers (Dacre et al. 2019), long-range moisture transport from the subtropics and tropics has an important share in the midlatitude moisture budget too (Knippertz and Wernli 2010; Sodemann and Stohl 2013; Norris et al. 2020; Guan et al. 2020). According to our results, such moisture most likely contributes to precipitation outside the centers of deep cyclones. Thus, extending the methodology introduced here to precipitation falling in different dynamical settings represents a promising avenue for further advancing our mechanistic understanding of the midlatitude water cycle.

Finally, recent studies based on measurements of stable water isotopes in water vapor and precipitation have shown that moisture uptakes over the ocean by cold and dry air are associated with a distinct isotope signature (Aemisegger 2018; Thurnherr et al. 2021). Combined with our mechanistic insights into the water cycling in cyclones, this provides guidance for further exploring the possibilities to use isotope signals recorded in ice cores to reconstruct past storm track variability.

Acknowledgments. Important inspiration for this study came from the Ph.D. thesis of Jana Čampa. We thank three anonymous reviewers for their insightful comments that helped to improve the manuscript. Furthermore, we acknowledge the ECMWF for providing access to the ERA5 dataset.

Data availability statement. The ERA5 data can be downloaded from the Copernicus Climate Service (https://climate.copernicus.eu/climate-reanalysis).

REFERENCES

Aemisegger, F., 2018: On the link between the North Atlantic storm track and precipitation deuterium excess in Reykjavik. *Atmos. Sci. Lett.*, **19**, e865, https://doi.org/10.1002/asl.865.

——, and L. Papritz, 2018: A climatology of strong large-scale ocean evaporation events. Part I: Identification, global distribution, and associated climate conditions. *J. Climate*, **31**, 7287–7312, https://doi.org/10.1175/JCLI-D-17-0591.1.

Binder, H., M. Boettcher, H. Joos, and H. Wernli, 2016: The role of warm conveyor belts for the intensification of extratropical cyclones in Northern Hemisphere winter. *J. Atmos. Sci.*, **73**, 3997–4020, https://doi.org/10.1175/JAS-D-15-0302.1.

Boutle, I., R. Beare, S. Belcher, A. Brown, and R. Plant, 2010: The moist boundary layer under a mid-latitude weather system. *Bound.-Layer Meteor.*, **134**, 367–386, https://doi.org/10.1007/s10546-009-9452-9.

Browning, K. A., 1990: Organization of clouds and precipitation in extratropical cyclones. *Extratropical Cyclones: The Erik Palmen Memorial Volume*, C. W. Newton and E. O. Holopainen, Eds., Amer. Meteor. Soc., 129–153.

——, and N. M. Roberts, 1994: Structure of a frontal cyclone. *Quart. J. Roy. Meteor. Soc.*, **120**, 1535–1557, https://doi.org/10.1002/qj.49712052006.

Bui, H., and T. Spengler, 2021: On the influence of sea surface temperature distributions on the development of extratropical cyclones. *J. Atmos. Sci.*, **78**, 1173–1188, https://doi.org/10.1175/JAS-D-20-0137.1.

Čampa, J., 2012: Potential vorticity and moisture in extratropical cyclones: climatology and sensitivity experiments. Ph.D. thesis, Johannes Gutenberg-Universität Mainz, 115 pp., https://openscience.ub.uni-mainz.de/bitstream/20.500.12030/2762/1/3497.pdf.

——, and H. Wernli, 2012: A PV perspective on the vertical structure of mature midlatitude cyclones in the northern hemisphere. *J. Atmos. Sci.*, **69**, 725–740, https://doi.org/10.1175/JAS-D-11-050.1.

Carrera, M. L., J. R. Gyakum, and D.-L. Zhang, 1999: A numerical case study of secondary marine cyclogenesis sensitivity to initial error and varying physical processes. *Mon. Wea. Rev.*, **127**, 641–660, https://doi.org/10.1175/1520-0493(1999)127<0641:ANCSOS>2.0.CO;2.

Catto, J. L., and S. Pfahl, 2013: The importance of fronts for extreme precipitation. *J. Geophys. Res. Atmos.*, **118**, 10 791–10 801, https://doi.org/10.1002/jgrd.50852.

——, C. Jakob, G. Berry, and N. Nicholls, 2012: Relating global precipitation to atmospheric fronts. *Geophys. Res. Lett.*, **39**, L10805, https://doi.org/10.1029/2012GL051736.

Chang, E. K. M., and S. Song, 2006: The seasonal cycles in the distribution of precipitation around cyclones in the western North Pacific and Atlantic. *J. Atmos. Sci.*, **63**, 815–839, https://doi.org/10.1175/JAS3661.1.

Coronel, B., D. Ricard, G. Rivière, and P. Arbogast, 2015: Role of moist processes in the tracks of idealized midlatitude surface cyclones. *J. Atmos. Sci.*, **72**, 2979–2996, https://doi.org/10.1175/JAS-D-14-0337.1.

Dacre, H. F., O. Martínez-Alvarado, M. A. Stringer, and D. A. Lavers, 2015: How do atmospheric rivers form? *Bull. Amer. Meteor. Soc.*, **96**, 1243–1255, https://doi.org/10.1175/BAMS-D-14-00031.1.

——, ——, and C. O. Mbengue, 2019: Linking atmospheric rivers and warm conveyor belt airflows. *J. Hydrometeor.*, **20**, 1183–1196, https://doi.org/10.1175/JHM-D-18-0175.1.

Davis, C. A., E. D. Grell, and M. A. Shapiro, 1996: The balanced dynamical nature of a rapidly intensifying oceanic cyclone. *Mon. Wea. Rev.*, **124**, 3–26, https://doi.org/10.1175/1520-0493(1996)124<0003:TBDNOA>2.0.CO;2.

de Vries, A. J., 2021: A global climatological perspective on the importance of Rossby wave breaking and intense moisture transport for extreme precipitation events. *Wea. Climate Dyn.*, **2**, 129–161, https://doi.org/10.5194/wcd-2-129-2021.

Dufour, A., O. Zolina, and S. K. Gulev, 2016: Atmospheric moisture transport to the Arctic: Assessment of reanalyses and analysis of transport components. *J. Climate*, **29**, 5061–5081, https://doi.org/10.1175/JCLI-D-15-0559.1.

Field, P. R., and R. Wood, 2007: Precipitation and cloud structure in midlatitude cyclones. *J. Climate*, **20**, 233–254, https://doi.org/10.1175/JCLI3998.1.

Fink, A. H., S. Pohle, J. G. Pinto, and P. Knippertz, 2012: Diagnosing the influence of diabatic processes on the explosive deepening of extratropical cyclones. *Geophys. Res. Lett.*, **39**, L07803, https://doi.org/10.1029/2012GL051025.

Giordani, H., and G. Caniaux, 2001: Sensitivity of cyclogenesis to sea surface temperature in the northwestern Atlantic. *Mon. Wea. Rev.*, **129**, 1273–1295, https://doi.org/10.1175/1520-0493(2001)129<1273:SOCTSS>2.0.CO;2.

Guan, B., D. E. Waliser, and F. M. Ralph, 2020: A multimodel evaluation of the water vapor budget in atmospheric rivers. *Ann. N. Y. Acad. Sci.*, **1472**, 139–154, https://doi.org/10.1111/nyas.14368.

Gyakum, J. R., and R. E. Danielson, 2000: Analysis of meteorological precursors to ordinary and explosive cyclogenesis in the western North Pacific. *Mon. Wea. Rev.*, **128**, 851–863, https://doi.org/10.1175/1520-0493(2000)128<0851:AOMPTO>2.0.CO;2.

Hawcroft, M. K., L. C. Shaffrey, K. I. Hodges, and H. F. Dacre, 2012: How much Northern Hemisphere precipitation is associated with extratropical cyclones? *Geophys. Res. Lett.*, **39**, L24809, https://doi.org/10.1029/2012GL053866.

Hersbach, H., and Coauthors, 2020: The ERA5 global reanalysis. *Quart. J. Roy. Meteor. Soc.*, **146**, 1999–2049, https://doi.org/10.1002/qj.3803.

Hoskins, B., and M. Pedder, 1980: The diagnosis of middle latitude synoptic development. *Quart. J. Roy. Meteor. Soc.*, **106**, 707–719, https://doi.org/10.1002/qj.49710645004.

Knippertz, P., and H. Wernli, 2010: A Lagrangian climatology of tropical moisture exports to the Northern Hemispheric extratropics. *J. Climate*, **23**, 987–1003, https://doi.org/10.1175/2009JCLI3333.1.

Kuo, Y.-H., and R. J. R. S. Low-Nam, 1991: Effects of surface energy fluxes during the early development and rapid intensification stages of seven explosive cyclones in the western Atlantic. *Mon. Wea. Rev.*, **119**, 457–476, https://doi.org/10.1175/1520-0493(1991)119<0457:EOSEFD>2.0.CO;2.

Laederach, A., and H. Sodemann, 2016: A revised picture of the atmospheric moisture residence time. *Geophys. Res. Lett.*, **43**, 924–933, https://doi.org/10.1002/2015GL067449.

Ludwig, P., J. G. Pinto, M. Reyers, and S. L. Gray, 2014: The role of anomalous SST and surface fluxes over the southeastern North Atlantic in the explosive development of Windstorm Xynthia. *Quart. J. Roy. Meteor. Soc.*, **140**, 1729–1741, https://doi.org/10.1002/qj.2253.

Madonna, E., H. Wernli, H. Joos, and O. Martius, 2014: Warm conveyor belts in the ERA-Interim dataset (1979–2010). Part I: Climatology and potential vorticity evolution. *J. Climate*, **27**, 3–26, https://doi.org/10.1175/JCLI-D-12-00720.1.

Naakka, T., T. Nygård, T. Vihma, J. Sedlar, and R. G. Graversen, 2019: Atmospheric moisture transport between mid-latitudes and the Arctic: Regional, seasonal and vertical distributions. *Int. J. Climatol.*, **39**, 2862–2879, https://doi.org/10.1002/joc.5988.

Neiman, P. J., and M. A. Shapiro, 1993: The life cycle of an extratropical marine cyclone. Part I: Frontal-cyclone evolution and thermodynamic air–sea interaction. *Mon. Wea. Rev.*, **121**, 2153–2176, https://doi.org/10.1175/1520-0493(1993)121<2153:TLCOAE>2.0.CO;2.

Norris, J. R., and Coauthors, 2020: The observed water vapor budget in an atmospheric river over the northeast Pacific. *J. Hydrometeor.*, **21**, 2655–2673, https://doi.org/10.1175/JHM-D-20-0048.1.

Nuss, W. A., 1989: Air–sea interaction influences on the structure and intensification of an idealized marine cyclone. *Mon. Wea. Rev.*, **117**, 351–369, https://doi.org/10.1175/1520-0493(1989)117<0351:ASIIOT>2.0.CO;2.

Papritz, L., and H. Sodemann, 2018: Characterizing the local and intense water cycle during a cold air outbreak in the Nordic seas. *Mon. Wea. Rev.*, **146**, 3567–3588, https://doi.org/10.1175/MWR-D-18-0172.1.

——, S. Pfahl, I. Rudeva, I. Simmonds, H. Sodemann, and H. Wernli, 2014: The role of extratropical cyclones and fronts for Southern Ocean freshwater fluxes. *J. Climate*, **27**, 6205–6224, https://doi.org/10.1175/JCLI-D-13-00409.1.

——, ——, H. Sodemann, and H. Wernli, 2015: A climatology of cold air outbreaks and their impact on air–sea heat fluxes in the high-latitude South Pacific. *J. Climate*, **28**, 342–364, https://doi.org/10.1175/JCLI-D-14-00482.1.

Peixoto, J., and A. H. Oort, 1992: *Physics of Climate.* American Institute of Physics, 520 pp.

Pfahl, S., and H. Wernli, 2012: Quantifying the relevance of cyclones for precipitation extremes. *J. Climate*, **25**, 6770–6780, https://doi.org/10.1175/JCLI-D-11-00705.1.

——, and M. Sprenger, 2016: On the relationship between extratropical cyclone precipitation and intensity. *Geophys. Res. Lett.*, **43**, 1752–1758, https://doi.org/10.1002/2016GL068018.

——, E. Madonna, M. Boettcher, H. Joos, and H. Wernli, 2014: Warm conveyor belts in the ERA-Interim dataset (1979–2010). Part II: Moisture origin and relevance for precipitation. *J. Climate*, **27**, 27–40, https://doi.org/10.1175/JCLI-D-13-00223.1.

Ralph, F. M., P. J. Neiman, G. N. Kiladis, K. Weickmann, and D. W. Reynolds, 2011: A multiscale observational case study of a Pacific atmospheric river exhibiting tropical–extratropical connections and a mesoscale frontal wave. *Mon. Wea. Rev.*, **139**, 1169–1189, https://doi.org/10.1175/2010MWR3596.1.

Raveh-Rubin, S., 2017: Dry intrusions: Lagrangian climatology and dynamical impact on the planetary boundary layer. *J. Climate*, **30**, 6661–6682, https://doi.org/10.1175/JCLI-D-16-0782.1.

Reed, R. J., and M. D. Albright, 1986: A case study of explosive cyclogenesis in the eastern Pacific. *Mon. Wea. Rev.*, **114**, 2297–2319, https://doi.org/10.1175/1520-0493(1986)114<2297:ACSOEC>2.0.CO;2.

——, M. T. Stoelinga, and Y.-H. Kuo, 1992: A model-aided study of the origin and evolution of the anomalously high potential vorticity in the inner region of a rapidly deepening marine cyclone. *Mon. Wea. Rev.*, **120**, 893–913, https://doi.org/10.1175/1520-0493(1992)120<0893:AMASOT>2.0.CO;2.

Rossa, A. M., H. Wernli, and H. C. Davies, 2000: Growth and decay of an extra-tropical cyclone's PV-tower. *Meteor. Atmos. Phys.*, **73**, 139–156, https://doi.org/10.1007/s007030050070.

Rudeva, I., and S. K. Gulev, 2011: Composite analysis of North Atlantic extratropical cyclones in NCEP–NCAR reanalysis data. *Mon. Wea. Rev.*, **139**, 1419–1446, https://doi.org/10.1175/2010MWR3294.1.

Sodemann, H., 2020: Beyond turnover time: Constraining the lifetime distribution of water vapor from simple and complex approaches. *J. Atmos. Sci.*, **77**, 413–433, https://doi.org/10.1175/JAS-D-18-0336.1.

——, and A. Stohl, 2013: Moisture origin and meridional transport in atmospheric rivers and their association with multiple cyclones. *Mon. Wea. Rev.*, **141**, 2850–2868, https://doi.org/10.1175/MWR-D-12-00256.1.

——, C. Schwierz, and H. Wernli, 2008: Interannual variability of Greenland winter precipitation sources: Lagrangian moisture diagnostic and North Atlantic Oscillation influence. *J. Geophys. Res.*, **113**, D03107, https://doi.org/10.1029/2007JD008503.

——, and Coauthors, 2020: Structure, process, and mechanism. *Atmospheric Rivers*, F. M. Ralph et al., Eds., Springer, 15–43.

Sorteberg, A., and J. E. Walsh, 2008: Seasonal cyclone variability at 70°N and its impact on moisture transport into the Arctic. *Tellus*, **60A**, 570–586, https://doi.org/10.1111/j.1600-0870.2008.00314.x.

Sprenger, M., and H. Wernli, 2015: The LAGRANTO Lagrangian analysis tool—Version 2.0. *Geosci. Model Dev.*, **8**, 2569–2586, https://doi.org/10.5194/gmd-8-2569-2015.

——, and Coauthors, 2017: Global climatologies of Eulerian and Lagrangian flow features based on ERA-Interim. *Bull. Amer. Meteor. Soc.*, **98**, 1739–1748, https://doi.org/10.1175/BAMS-D-15-00299.1.

Stoelinga, M. T., 1996: A potential vorticity-based study of the role of diabatic heating and friction in a numerically simulated baroclinic cyclone. *Mon. Wea. Rev.*, **124**, 849–874, https://doi.org/10.1175/1520-0493(1996)124<0849:APVBSO>2.0.CO;2.

Sutcliffe, R. C., 1947: A contribution to the problem of development. *Quart. J. Roy. Meteor. Soc.*, **73**, 370–383, https://doi.org/10.1002/qj.49707331710.

Tamarin, T., and Y. Kaspi, 2016: The poleward motion of extratropical cyclones from a potential vorticity tendency analysis. *J. Atmos. Sci.*, **73**, 1687–1707, https://doi.org/10.1175/JAS-D-15-0168.1.

Thurnherr, I., and Coauthors, 2021: The role of air–sea fluxes for the water vapour isotope signals in the cold and warm sectors of extratropical cyclones over the Southern Ocean. *Wea. Climate Dyn.*, **2**, 331–357, https://doi.org/10.5194/wcd-2-331-2021.

Tilinina, N., A. Gavrikov, and S. K. Gulev, 2018: Association of the North Atlantic surface turbulent heat fluxes with midlatitude cyclones. *Mon. Wea. Rev.*, **146**, 3691–3715, https://doi.org/10.1175/MWR-D-17-0291.1.

Trenberth, K., and C. Guillemot, 1998: Evaluation of the atmospheric moisture and hydrological cycle in the NCEP/NCAR reanalyses. *Climate Dyn.*, **14**, 213–231, https://doi.org/10.1007/s003820050219.

Uccellini, L. W., 1990: Processes contributing to the rapid development of extratropical cyclones. *Extratropical Cyclones: The Erik Palmen Memorial Volume*, C. W. Newton and E. O. Holopainen, Eds., Amer. Meteor. Soc., 81–105.

Vannière, B., A. Czaja, H. Dacre, and T. Woollings, 2017: A ''cold path'' for the Gulf Stream–troposphere connection.

J. Climate, **30**, 1363–1379, https://doi.org/10.1175/JCLI-D-15-0749.1.

Wernli, H., 1997: A Lagrangian-based analysis of extratropical cyclones. II: A detailed case-study. *Quart. J. Roy. Meteor. Soc.*, **123**, 1677–1706, https://doi.org/10.1002/qj.49712354211.

——, and H. C. Davies, 1997: A Lagrangian-based analysis of extratropical cyclones. I: The method and some applications. *Quart. J. Roy. Meteor. Soc.*, **123**, 467–489, https://doi.org/10.1002/qj.49712353811.

——, and C. Schwierz, 2006: Surface cyclones in the ERA-40 dataset (1958–2001). Part I: Novel identification method and global climatology. *J. Atmos. Sci.*, **63**, 2486–2507, https://doi.org/10.1175/JAS3766.1.

Winschall, A., S. Pfahl, H. Sodemann, and H. Wernli, 2014a: Comparison of Eulerian and Lagrangian moisture source diagnostics—The flood event in eastern Europe in May 2010. *Atmos. Chem. Phys.*, **14**, 6605–6619, https://doi.org/10.5194/acp-14-6605-2014.

——, H. Sodemann, S. Pfahl, and H. Wernli, 2014b: How important is intensified evaporation for Mediterranean precipitation extremes? *J. Geophys. Res. Atmos.*, **119**, 5240–5256, https://doi.org/10.1002/2013JD021175.

Zolina, O., and S. K. Gulev, 2003: Synoptic variability of ocean–atmosphere turbulent fluxes associated with atmospheric cyclones. *J. Climate*, **16**, 2717–2734, https://doi.org/10.1175/1520-0442(2003)016<2717:SVOOTF>2.0.CO;2.